SPREADING, SOLIDIFICATION AND REMELTING BEHAVIOR OF LIQUID METAL DROPLETS SEQUENTIALLY IMPINGING ONTO A METAL SUBSTRATE

by

LISTER MANOHAR PINTO

Presented to the Faculty of the Graduate School of

The University of Texas at Arlington in Partial Fulfillment

of the Requirements

for the Degree of

MASTER OF SCIENCE IN MECHANICAL ENGINEERING

THE UNIVERSITY OF TEXAS AT ARLINGTON

August 2005

DEDICATION

To my parents, who have made numerous sacrifices, borne suffering and devoted the better part of their lives to make me all that I am. I love you, Mom and Dad.

ACKNOWLEDGEMENTS

I take this opportunity to acknowledge the contributions of a select few, without whom this research would not have been possible.

First and foremost, Dr. Albert Y. Tong, who served as not only my advisor, but my guide and mentor through the three semesters I have worked with him. He made himself available to me through personal contact, phone and e-mail, round the clock throughout the year. His diligence and supervision have been the driving force behind the work presented in this thesis.

Zhaoyuan Wang, who introduced me to the intricacies of the flow-solver and the procedure involved in post-processing the data, was always open to questions and more often than not was able to provide adequate answers, and one to whom I am greatly indebted.

Barbara Howser, Librarian assigned to the Department of Mechanical Engineering, who helped me gain access to all literature required for my reference and provided assistance throughout my research.

And finally, the Department of Mechanical & Aerospace Engineering at the University of Texas at Arlington, whose fellowship and financial assistance allowed me to concentrate on the development and completion of this research.

April 25, 2005

ABSTRACT

SPREADING, SOLIDIFICATION AND REMELTING BEHAVIOR
OF LIQUID METAL DROPLETS SEQUENTIALLY
IMPINGING ONTO A METAL
SUBSTRATE

Publication No. _____

Lister Manohar Pinto, M.S.

The University of Texas at Arlington, 2005

Supervising Professor: Albert Y. Tong

The fluid dynamics and simultaneous solidification of two successive molten metal droplets impacting a flat substrate is investigated numerically. The primary objective is to investigate the effects of initial droplet and substrate temperature, and the latent heat of substrate material, on the spreading, solidification and remelting of molten tin droplets impacting a substrate of the same material. A robust fluid-flow solver that is capable of modeling rapidly deforming free surfaces involving a moving phase-change boundary is employed in the study. The Navier-Stokes equations are solved using a finite volume formulation. A two-step projection method is used to solve for

incompressible flow. The free surfaces of the droplets are tracked by the volume-of-fluid method with a second order accurate piecewise linear scheme. The surface tension force is modeled by the continuum surface flow model. The energy equation is modeled using an enthalpy-based formulation.

The predictive model used in this study enables the optimization of operating parameters to reveal impinging droplet temperatures and initial substrate temperatures that promote substrate remelting, possess good flow characteristics and yet, minimize thermally induced stresses and excessive remelting of previously deposited material. The results of this investigation are relevant to droplet deposition technologies involving large diameter droplets at low velocities.

TABLE OF CONTENTS

Appendix

LIST OF ILLUSTRATIONS

LIST OF TABLES

CHAPTER 1

INTRODUCTION

1.1 Motivation

The solidification, heat and fluid flow during the impact of a single droplet on a substrate are complex phenomena. Droplet spreading is a free surface problem with large domain deformations in the presence of surface tension. The associated transient heat transfer process involves convection with large temperature gradients in a deforming domain, liquid spreading constrained by the multidimensional advancement of solidification interface, as well as the extraction of heat from a diminishing liquid region that is coupled with conduction in the substrate. The coupling between solidification and fluid dynamics can lead to non-intuitive shapes. Experimental investigations of droplet impingement and solidification are also quite challenging, due to the very fast flow and thermal transients as well as the small length scales involved, in the order of milliseconds and millimeters, respectively. Due to the above mentioned difficulties, numerical modeling becomes necessary to provide insight into the relative importance of the various process parameters such as the initial temperature of the droplet and substrate, and material properties such as latent heat of the substrate.

The interest in studying droplet impingement and solidification stems from its application to novel methods of manufacturing. These methods are discussed next.

1.2 Manufacturing Applications

On the basis of the application of the process, droplet impingement processes can be broadly classified into coating processes and forming processes. Coating processes involve application of a layer on the base material to impart to it desired protective and aesthetic properties. Forming processes involve deposition of parent material onto a substrate or sacrificial material, with the intention of manufacturing a new artifact with desired geometry.

Droplet impingement technologies can also be classified into spraying and deposition processes. Spraying involves impingement of small diameter droplets at high velocities. On the contrary, deposition processes involve large diameter droplets at much lower velocities.

Although most current innovations involving droplet impingement fall into either of the above categories, each is distinguished by certain characteristic features. A brief description for each is provided below.

1.2.1 Shape Deposition Manufacturing (SDM)

Shape Deposition manufacturing is a process for automatically fabricating complex multi-material objects by sequentially depositing material layers. Microcasting [1,2] is a molten metal droplet deposition process in SDM, which is able to create fully dense metal layers with controlled microstructure. In the microcasting process, an arc is established between a conventional plasma welding torch and a feedstock wire which is supplied from a charged contact tip. Deposition material melts in the arc and free falls

in the form of discrete droplets from the wire. Accelerated by gravity, the droplets, whose diameter is of the order of millimeters, flatten upon impact with the substrate.

In microcasting SDM, objects are incrementally built-up using a combination of layered material deposition and removal as shown in Figure 1.1. Individual layers are deposited by a robot arm as a sequence of rows in a prescribed pattern formed by individual droplets of superheated molten metal. Layers are then accurately machined to net shape before depositing additional material. Microcasting SDM has been used to deposit several metals including carbon steel, stainless steel, copper, aluminum, bronze and invar.

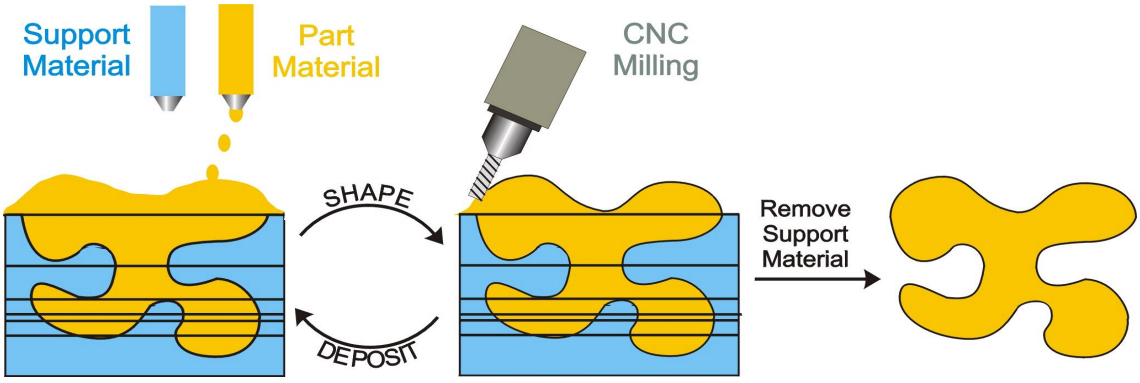

Figure 1.1 Schematic of the microcasting process [2]

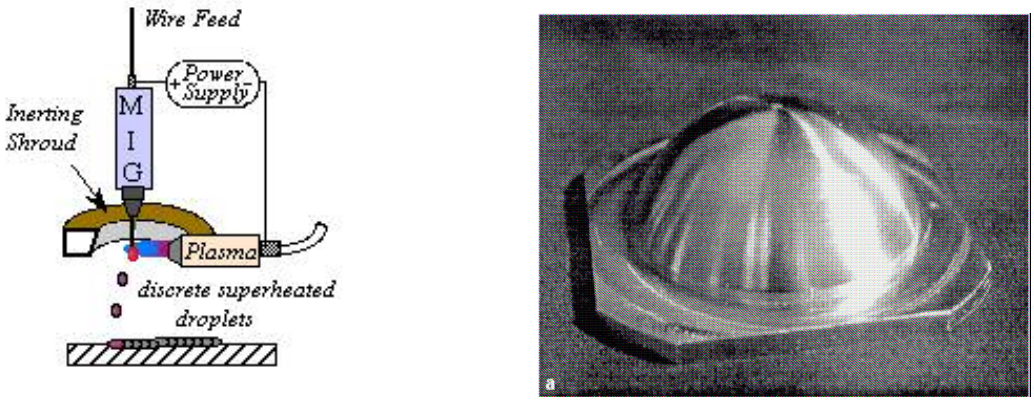

Figure 1.2 Method of droplet delivery (left) and a structure [2] built by SDM (right)

1.2.2 Picoliter Size Droplet Dispensing

Picoliter size droplet dispensing [3-5] is used for advanced Surface Mount Technologies (SMT). A central example of an application of such a technology is chip packaging in microelectronics. Scale reduction of such packages has predominantly been achieved by replacing wire connections from electrical connector pads by monodispersed arrays of solder microdroplets (25 – 100 μm in diameter) which are printed on a substrate. These microdroplets, also known as bumps, feature a smaller pitch size, form an electrical connection and allow for higher connector densities. Important advantages of picoliter size droplet dispensing over other bumping technologies are flexibility and low cost, because neither masks nor screens are required.

1.2.3 Thermal Spray Coating

Surface properties of a component can be modified by depositing a thin layer of different material on it. One widely used technique of applying such surface layers is thermal spray coating [6,7]. Thermal spray coating is an elevated temperature, high velocity material processing technique in which metal or ceramic particles are melted in a hot flame or plasma, and the melt is accelerated towards the target material or substrate, where they rapidly solidify and form a layered deposit. Thermal spray coatings have found applications in diverse areas such as corrosion protection, wear resistance, thermal barriers, high temperature oxidation protection and functional surfaces.

1.2.4 Digital Microfabrication

Objects, materials or components maybe built up by precise deposition of molten microdrops under controlled thermal conditions. This provides a means of digital microfabrication [8], or fabrication of 3D objects such as electronic circuits, microdrop by microdrop under complete computer control much in the same way as 2D hard copy is obtained by ink-jet printing. The letters 'MIT' in Figure 1.3 are about 300 μm tall and stand upright from a plastic surface. They are fabricated by precise deposition of molten microdrops from above, each droplet solidifying by heat transfer to the ambient air before the next one arrives. The molten material is wax and the droplets are 50 μm in diameter, but in principle the process can be used with other melts as well.

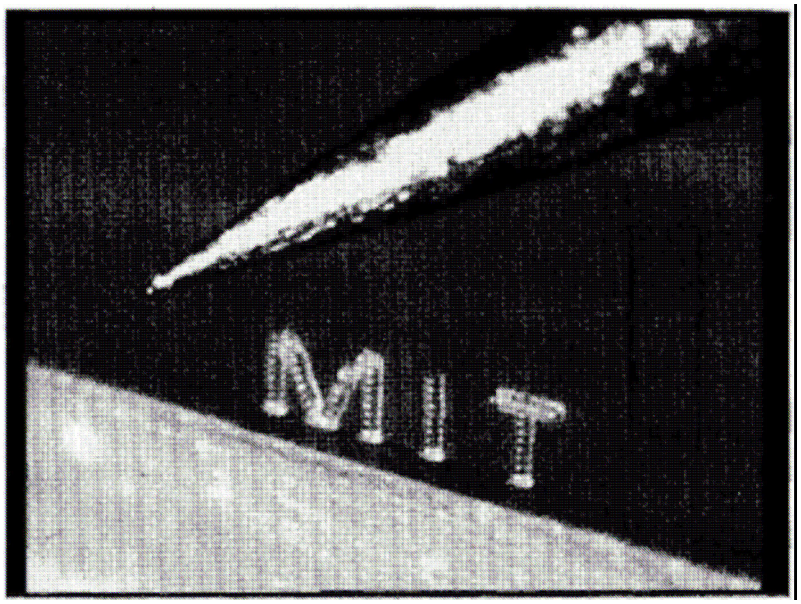

Figure 1.3 Freestanding 300 μm tall letters produced by dropwise deposition of molten wax microdrops. The conical object is the tip of a common pin; the rectangle measures 200 μm x 600 μm [8]

1.2.5 Liquid Metal Jetting (LMJ)

Liquid Metal Jetting [9] is a solid freeform fabrication process for producing metal mechanical parts and electronic interconnects. Similar to ink jet printing, LMJ is a technology in which individual molten droplets are accurately printed. LMJ seeks to produce metal parts on demand from a CAD database with functional performance parameters similar to metal parts produced by machining or casting. By controlling solidification rates and metal alloy composition, LMJ is able to produce parts with unique properties such as metal matrices and functionally graded materials. Figure 1.4 provides a schematic view of the overall process.

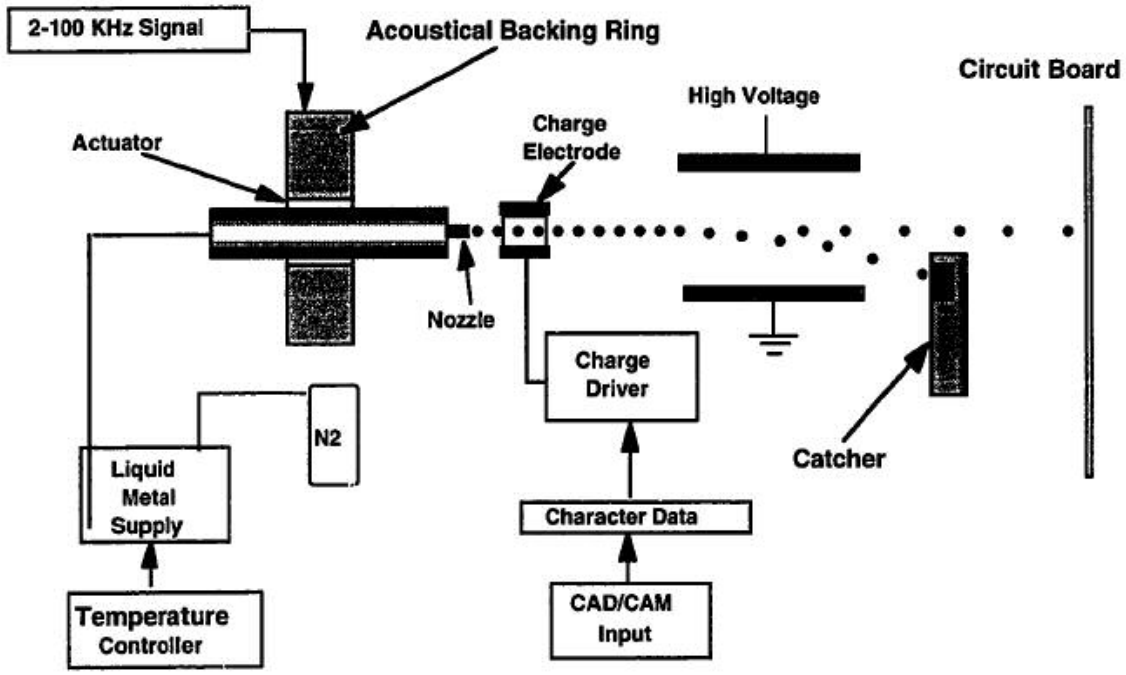

Figure 1.4 Jet dispensing system [10]

1.2.6 Precision Droplet-based Net-form Manufacturing (PDM)

The crux of the PDM technique [11] lies in the ability to generate highly uniform streams of molten metal droplets such as aluminum or aluminum alloys. A conceptual schematic of the PDM process is shown in Figure 1.5. Droplets are generated from capillary stream break-up in an inert environment and are predeposited onto a substrate whose motion is controlled by a programmable x-y table. In this way, tubes with circular, square and triangular cross sections have been fabricated as illustrated in the figure below.

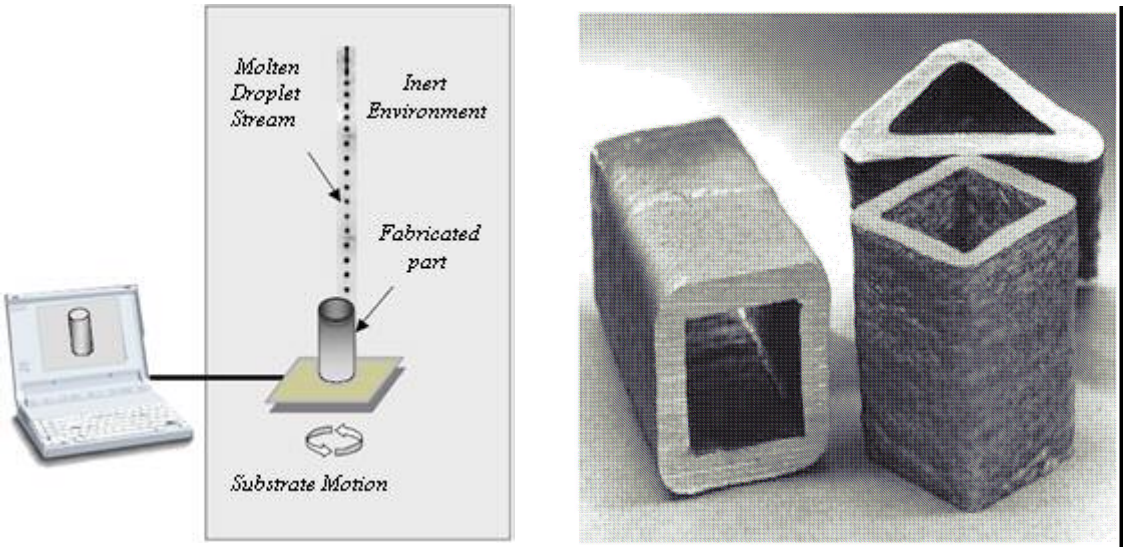

Figure 1.5 Conceptual schematic of component fabrication (left), and fabricated components [11] (right)

1.3 Literature Review

Over the past decade, a vast body of literature pertaining to the dynamics of single molten droplet impingement has been published. Among the pioneering works of research in the area of droplet impingement dynamics is that of Madejski [12,13], who

examined solidification of droplets on a cold solid surface. A simple model of radial two-dimensional flow was employed, and a theoretical and experimental analysis performed. The initial shape of the splat was considered to be a cylinder, a simplifying assumption. The solution of the Stefan problem, which was the starting point for many models at that time, was utilized in the development of the theory. The degree of flattening, now commonly referred to as the spread factor, was found to be a function of Weber, Reynolds and Peclet number, thus tying the influence of viscous dissipation, surface tension, convection and diffusion into the overall impingement and solidification process.

Collings et al. [14] observed solidified splats of the alloy Nitronic 40W, and made a commendable attempt to explain the shape of the splats accompanied by a limited theoretical analysis. Further, the work of Madejski was reviewed and a number of possible improvements to the model were presented, one of which was the extension of the heat transfer analysis to depart from the assumption of ideal heat transfer at the splat-substrate interface, and to include the effects release of latent of fusion at the advancing solid-melt interface.

Trapaga et al. [15] developed a mathematical representation of the spreading and solidification process of a single droplet impacting on a substrate. A fairly comprehensive numerical analysis was conducted and substantiated with experimental results. Droplet size and velocity were found to influence the spreading-solidification behavior. However, the model did not include the interaction of the droplet with the substrate, a feature that would be needed to be incorporated to achieve a more realistic

picture of the solidification phenomena. Almost concurrently, Bennett and Poulikakos [16] attempted to segregate the effects of surface tension and viscosity on the solidification process into different regimes. Two domains characterized by the Weber and Reynolds number were defined, each representing the regimes where the surface tension and viscous dissipation respectively, dominated the termination of the spreading of the splat. It was concluded that solidification effects were secondary to the effects of surface tension and viscous dissipation in arresting the spreading of the droplet.

Liu et al. [17] employed Madejski's analysis of the solidification process and solved the Navier-Stokes equations to obtain a numerical model to simulate the droplet impingement and subsequent solidification process for single and multiple droplets, with emphasis laid on process parameters encountered in plasma spraying. The substrate was assumed to be isothermal in this approach. Droplet and substrate temperature effects, as well as impact velocity effects were studied. The model suffered from the errors inherent in Madejski's model due to assumptions such as semi-infinite substrate and splat regions, and constant contact temperatures, which are valid only under certain limiting conditions.

Kang et al. [18] developed a very primitive model of droplet impingement and heat transfer, decoupling the two effects and assuming cylindrical shapes for the initial splats. Sequential impact of two droplets was studied. The theoretical analysis accounted for slower cooling rates of second droplet compared to the first, and also for the two dimensional temperature field in the substrate. The importance of including the contact resistance in the model was also highlighted. The model was later extended to

account for remelting [19] of the first splat by the second. No attempt was made to improve on the weaknesses of the earlier model. Heat conduction was considered one-dimensional, neglecting the radial conduction. Initial shapes of the splats were assumed to be cylindrical discs, thereby totally disregarding the process of deformation accompanying the impingement process. The degree of remelting was found to vary with the amount of superheat as well as thermophysical properties such as latent heat and melting temperature.

Perhaps the most comprehensive analytical study on single molten droplet deposition was developed by Gao and Sonin [8]. The results were with regards to digital microfabrication, and included expressions for various thermal and solidification timescales, solidification angles and conditions to avoid in-flight droplet break-up. Gravitational effects on the impact process were found to be insignificant. However, most of the results were obtained under conditions where droplet deposition occurred on a much shorter timescale than solidification. Subsequently, Schiaffino and Sonin [20] studied molten droplet deposition and solidification phenomena at low Weber numbers. Based on experiments for various regimes, correlations were derived for spreading velocity and spreading timescales. In homologous deposition, where the droplet and target are of the same material, the spread factor was obtained as a function of the Stefan number.

Amon et al. [1] investigated the interface bonding via substrate remelting of an impinging molten droplet in the microcasting process. The model developed for the study decoupled one-dimensional heat transfer from the fluid dynamics, and assumed

the absence of effects of contact resistance and convection heat transfer. Stefan's solution was used to obtain the location of the melting front. The results obtained include the prediction of droplet temperature necessary to cause remelting. Along similar lines, Chin et al. [21] studied the effect of substrate preheating on the residual stresses induced in microcasting and concluded that moderate levels of preheating significantly reduce the stresses in the substrate. In a later study, Zarzalejo et al. [2] reported that neglecting heat transfer due to forced convection underestimated remelting depths and the occurrence of remelting. An attempt was made to incorporate the effects of convection by introducing an effective thermal conductivity achieved by multiplying the liquid conductivity by a factor greater than unity. A numerical model using the Spectral Element Method was developed and used to model the remelting behavior. A parametric study by Schmaltz et al. [22] revealed that preheating the substrate facilitated the remelting process. Solidification times were found to increase when either the droplet or substrate temperatures were increased.

Zhao et al. [3,23] modeled the heat transfer and fluid dynamics during the collision of a liquid droplet on a substrate, both numerically and experimentally. The numerical model was based on Lagrangian formulation and was solved using the finite element method. The thermal interaction of the droplet with the substrate was not included in the analysis. The study questions the validity of the varying timescales for spreading and solidification, and highlights the radial nature of temperature variations in the substrate, as well as the effects of droplet velocity and diameter on the spread factor.

Rangel and Bian [24] presented a metal-droplet deposition model to describe liquid deformation and to study substrate remelting. However, the initial shape of the splat was assumed as a cylindrical disc, and radial conduction was neglected. Nevertheless, the model was able to capture the effects of various parameters on the spread factor and solidification time of the droplet. Increase in the impact velocity was found to result in an increase in spread factor and decrease in the solidification time. An increase in diameter of the droplet however, led to an increase in both the spread factor and the solidification time. Remelting was found to occur when the substrate was sufficiently preheated, and solidification times were found to increase when remelting occurred.

A significant development came in the form of an independent work of research carried out by Tong and Holt [25]. The energy equations were coupled with the Navier-Stokes equations and solved using a finite volume formulation. The energy equations were solved using the enthalpy method and integrated with a previously developed fluid-flow solver. The droplet was assumed to impinge on an isothermal surface maintained below the melting point of the droplet. Both non-solidifying and solidifying cases were studied. The effects of impact velocity, droplet diameter, substrate temperature, specific heat and thermal conductivity on the spread factor was studied and found to be in agreement with available data. The effect of thermal contact resistance was also studied and consequently implemented into the numerical model.

An extension to the above study was conducted by Lu [26], who implemented a more robust free-surface tracking scheme into the numerical model. The flexibility of

studying molten droplet impingement with or without interaction with the substrate was also incorporated. The improved model was utilized to study different phenomena such as two-droplet collision, jet impingement and single droplet impingement. The objective of the study was, however, to validate the free-surface tracking scheme and no particular emphasis was laid on the study of dynamics of single droplet impingement.

Dynamics of the single droplet impingement with substrate remelting was the focus of a later study [27] which used the code improved by Lu. The effect of thickness and temperature of substrate, and of diameter, velocity and temperature of the droplet, on the remelt depth was investigated. An increase in all the aforementioned parameters with the exception of the substrate thickness were found to result in an increase in remelt depth.

Similar studies using numerical codes containing features akin to those implemented by Holt and Lu have been employed to study impingement of molten droplets of various materials with regards to a number of deposition processes. Pasandideh-Fard et al. [28] studied the impact of tin droplets on stainless steel numerically and corroborated the veracity of the simulations by comparing with experimental results. Predictions of maximum splat diameter were found sensitive to the assumed value of contact resistance. An analytical model was also developed to estimate maximum splat diameter. The effect of solidification on droplet impact dynamics was found to be negligible if $\sqrt{Ste/Pr} << 1$.

Fukai et al. [29] presented a finite element model to study the effect of solidification on the spread of tin droplets impinging onto a substrate. The model

predicted the dependence of spread factor on the Weber number and highlighted the importance of the role played by the frozen layer at the splat edge in arresting the spreading.

The results of a numerical investigation conducted by Attinger and Poulikakos [30], into the behavior of molten microdroplet impact onto a substrate underlined the importance of fluid dynamics on the substrate melting phenomenon. The numerical model was based on the axisymmetric Lagrangian finite element formulation of the Navier-Stokes equation. The influence of thermal and hydrodynamic initial conditions on the amount of substrate melting was discussed for a range of superheat and impact velocity. The melted volume (volume of melted material in the substrate) was found to increase with increasing superheat and impact velocity.

As is evident from the review of published literature, experimental results pertaining to axisymmetric and sequential impingement of two liquid molten droplets are limited, if not non-existent. The majority of the numerical analyses on the problem of axisymmetric multiple molten droplet impingement are primitive, to say the least. The models used are either applied to conditions involving assumptions that result in over-simplification, or the models themselves contain inadequacies that severely limit their ability to realistically model the problem. The focus of this research is to address the above issues.

1.4 Thesis Objective

The primary objective of this research is to investigate the effects of important process parameters and material properties on the solidification and remelting behavior

of liquid metal droplets sequentially impinging onto a substrate. To this end, parametric studies are conducted to highlight the influence of initial droplet and substrate temperature, and the latent heat of substrate material, on the spreading, solidification and remelting of molten tin droplets impacting a substrate of the same material. The results of this investigation are relevant to droplet deposition technologies involving large diameter droplets at low velocities. The predictive model used in this study enables the optimization of operating parameters to create impinging droplet temperatures that promote substrate remelting, possess good flow characteristics, and yet, minimize thermally induced stresses and excessive remelting of previously deposited material.

1.4 Thesis Outline

The following chapters aim to present a holistic picture of the numerical model, achieve an understanding of the underlying theory, document the procedure involved in setting up the problem and obtaining the solution, and illustrate graphically the influence of studied parameters on the spreading, solidification and remelting behavior of molten tin droplets impinging onto a tin substrate.

Chapter 2 seeks to delineate the challenges faced in constructing a model to simulate free-surface flows involving phase change and presents an overview of the governing equations and assumptions made in the development of the model used in this study.

Chapter 3 proceeds to outline the manner in which the problem is setup; important variables involved are elucidated and their significance highlighted. Matters such as selection of grid spacing and boundary conditions are covered in this chapter.

Chapter 4 serves to present the results obtained via numerical simulation and illustrate graphically the effect of various parameters on the spread factor, solidification time and remelt depth. An attempt is made to offer credible explanations for the physics underlying the variations observed.

Based on these explanations, conclusions are arrived at and summarized in Chapter 5. The scope for improvements to the present model, as well as the application of the obtained results to manufacturing is enumerated at the end of the chapter.

CHAPTER 2

NUMERICAL FORMULATION

2.1 Numerical Modeling

Numerical simulation of impact and solidification phenomena is a challenging proposition. The complexities include the dynamics of a rapidly moving free surface, the importance of both convective and diffusive energy transfer, and the existence of a liquid/solid phase-change boundary. The moving free surface has long proven to be a difficult problem because it entails the determination of the location of the boundary, which is unknown, and at the same time is desired as part of the solution. The difficulty is that the droplet surface deforms while the values of the field variables are being solved. From a computational standpoint, this presents some very serious issues depending on the solution method used. For example, if the free surface does not coincide with grid points, interpolation or some other means must be used to locate or approximate the free surface. It is imperative to exercise care so that numerical errors do not become excessive. Due to the rapid deformation of the droplet during the impact process, both convective and diffusive energy transfers are important and must be included in the energy equation. Finally, the modeling of a phase change shares many of the difficulties of the free surface. It also requires the accounting of the latent heat of fusion in the energy equation.

Two methods have been developed to cope with the boundary which is free to move in space and with time. One is the moving grid method, where the computational domain deforms with the moving surface. This method is a Lagrangian concept, in which the observer moves along with the falling droplet. Here, the droplet domain is fitted with a mesh using, for example, a boundary-fitted coordinate system or an unstructured grid. The free surface coincides with the mesh boundary and no interpolation among the grid points for the free surface is needed.

The other method is the fixed grid method, where stationary grids are used to keep track of what passes through each of the computational cells. This method is an Eulerian approach where the droplet falls past a stationary observer. A family of computer codes using the fixed grid method has been developed at the Los Alamos National Laboratory. The first in this series was called the Marker and Cell Method (MAC) [31], developed in 1966. The MAC method was succeeded by the Solution Algorithm (SOLA) [32] in 1975 and the Volume-Of-Fluid method (SOLA-VOF) [33] in 1980. They were followed by VOF-2D [34] in 1985, and finally RIPPLE [35] in 1991. This family of computer codes has been systematically improved over the years to better simulate flows with free surfaces. RIPPLE has been refined to include effects of surface tension on free surfaces in two-dimensional or three-dimensional axisymmetric geometry. Also, the domain can contain obstacles that the fluid must flow around. These obstacles can fill all or only part of a computational cell. Surface tension at free surfaces is replaced by a volume force derived from the continuum surface force (CSF) model [36]. A two-step projection method is used to solve for incompressible

flow, a method in which the pressure Poisson equation (PPE) is solved via a robust incomplete Cholesky conjugate gradient (ICCG) technique [37]. RIPPLE does not, however, incorporate modeling of heat transfer effects, nor does it have any provision for following a moving phase-change boundary.

The existence of phase change in the numerical calculations poses a challenge because it is a mathematical discontinuity. During a phase-change process, a large amount of energy is released or absorbed, creating a jump discontinuity in the energy dissipation. There are two popular approaches to the solution of this problem: the Stefan approximation, designed to predict the precise location of the phase-change front and, the enthalpy method, used when the phase-change front is known to occur within a known interval. The Stefan formulation is used when the location of the solid/liquid boundary is important. This formulation requires the use of a deforming grid or transformed coordinate system. The enthalpy formulation is attractive in cases where phase change may constitute only part of the complex problem. This formulation allows a fixed grid to be used in the solution. Also, it removes the need to explicitly satisfy conditions at the phase-change front, thus making it suitable for use in standard solution procedures. A recent review on the numerical simulation of convective/diffusion phase change problems is given in [38].

For the purpose of the present study, a version of the RIPPLE code modified by Holt [10], who incorporated an enthalpy-based formulation of the energy equation which includes both convection-diffusion heat transfer and a mushy-region for the

phase change, has been employed. The modified code provides a realistic model for the dynamic and thermal aspects of the impact process.

2.2 Assumptions

In the modeling of sequential impingement of two molten droplets, the following assumptions and approximations are made:

1. The droplets are assumed to be initially spherical and of equal diameters. Current droplet deposition technologies enable deployment of uniform sized droplets on a consistent basis. Deformation in the droplets as they are accelerated to the substrate is considered to be negligible since the size of the droplets is small (of the order of 1mm).

2. The free surface of the droplet is assumed to be adiabatic, i.e. the free surface is insulated from the ambient, and heat transfer is from the droplet to the substrate. This approximation is valid since the dominant heat transfer mode is conduction to the substrate.

3. The variation of material properties such density and viscosity are modeled as independent of the temperature.

4. The thermal and fluid properties of the droplet material in solid and liquid states are the same. This assumes that the difference in the magnitude of the solid and liquid properties is small, and does not give rise to any significant errors.

5. A constant value of thermal contact resistance and contact angle is used for the entire simulation.

2.3 Governing Equations

The numerical scheme in the flow solver used in this study is based on a finite difference solution of a coupled set of partial differential equations governing incompressible fluid flow. A review of the governing equations and the finite difference expressions used to approximate the governing equations is presented in brief, for completeness.

For incompressible fluids, the continuity equation is given by

$$\nabla \cdot \vec{V} = 0 \tag{1}$$

and the momentum equation is given by

$$\frac{\partial \vec{V}}{\partial t} + \nabla \cdot (\vec{V}\vec{V}) = -\frac{1}{\rho}\nabla p + \frac{1}{\rho}\nabla \cdot \tau + \vec{g} + \frac{1}{\rho}\vec{F}_b \tag{2}$$

For Newtonian fluids, we have:

$$\tau = 2\mu S \quad \text{and} \quad S = \frac{1}{2}[(\nabla \vec{V}) + (\nabla \vec{V})^T] \tag{3}$$

where S is the rate-of-strain tensor. The momentum equation expressed above is approximated with a finite-difference in time as

$$\frac{\vec{V}^{n+1} - \vec{V}^n}{\delta t} = -\nabla \cdot (\vec{V}\vec{V})^n - \frac{1}{\rho^n}\nabla p^{n+1} + \frac{1}{\rho^n}\nabla \cdot \tau^n + \vec{g}^n + \frac{1}{\rho^n}\vec{F}_b^n \tag{4}$$

where the superscripts n and n+1 represent the value of the variable at consecutive time steps. It is decomposed into the following two equations:

$$\frac{\tilde{\vec{V}} - \vec{V}^n}{\delta t} = -\nabla \cdot (\vec{V}\vec{V})^n + \frac{1}{\rho^n}\nabla \cdot \tau^n + \vec{g}^n + \frac{1}{\rho^n}\vec{F}_b^n \tag{5}$$

and

$$\frac{\vec{V}^{n+1} - \vec{\tilde{V}}}{\delta t} = -\frac{1}{\rho^n}\nabla p^{n+1} \tag{6}$$

where $\vec{\tilde{V}}$ represents an intermediate value of the velocity.

The two-step projection method is used to obtain a solution for the system of Eqs. (1) and (2). In the two-step projection method, a time discretization of the momentum equation, Eq. (4), is broken up into two equations, Eqs. (5) and (6). In the first step, an intermediate velocity field $\vec{\tilde{V}}$, is computed from Eq. (5) which accounts for incremental changes resulting from viscosity, advection, gravity, and body forces. In the second step, the velocity field $\vec{V}^{n+1}$, is projected onto a zero-divergence vector field resulting in a single Poisson equation for the pressure field given by

$$\nabla \cdot \left[\frac{1}{\rho^n}\nabla p^{n+1} \right] = \frac{\nabla \cdot \vec{\tilde{V}}}{\delta t} \tag{7}$$

which is solved by using an incomplete Cholesky conjugate gradient solution technique.

Free surfaces need to be tracked and reconstructed. In the flow solver used here, Volume-of-Fluid method is used to track the free surface. The VOF technique provides a means of following fluid regions through an Eulerian mesh of stationary cells, and was developed by Hirt and Nichols [39]. The basis of the VOF method is the fractional volume-of-fluid scheme for tracking free boundaries. The governing equation in this method is given by

$$\frac{DF}{Dt} = \frac{\partial F(\vec{x},t)}{\partial t} + \vec{V} \cdot \nabla F(\vec{x},t) = 0 \tag{8}$$

where F is defined as the volume fraction of fluid whose value is unity at any point occupied by fluid and zero elsewhere. In particular, a unit value of F corresponds to a cell full of fluid, whereas a zero value indicates that the cell contains no fluid. A cell with F values between zero and one contains a free surface. When averaged over a computational cell, F is equal to the fractional volume of the cell occupied by fluid. In addition to defining which cells contain a boundary, the F function can be used to determine the fluid location within a boundary cell.

The Nichol-Hirt VOF scheme utilizes a piecewise-constant interface to reconstruct the interface. In the present study, this scheme has been replaced by a more robust Youngs' VOF scheme [40], which uses a piecewise-linear interface. The original paper by Youngs had little detail of the methods by which the interface was reconstructed and fluxes calculated. The algorithm outlined by Rudman [41] for the Youngs' VOF scheme has been implemented into the code.

A non-conventional approach referred to earlier, called the Continuum Surface Force (CSF) method is used to model surface tension. The CSF method interprets surface tension as a continuous, three-dimensional effect across an interface rather than a boundary value condition at the interface. Interfaces between fluids of different properties (called colors) are represented as transition regions of finite thickness. Across this region there is a continuous variation of the property value of one fluid to the property value of the other fluid. A force density, which is proportional to the curvature of the surface of constant property at the point, is defined at each point in the transition region. It is also normalized so that the conventional description of the surface tension

on an interface is recovered when the ratio of local transition region thickness to local radius of curvature approaches zero.

Holt employed an algorithm developed by Voller et al. [42] to model heat transfer effects and to track a moving phase-change boundary. Heat transfer is governed by an enthalpy-based energy equation given by

$$\frac{\partial \rho h}{\partial t} + \nabla \cdot (\rho \vec{V} h) - \nabla \cdot (\alpha \nabla h) - S_h = 0 \qquad (9)$$

where $\alpha = k/Cp$ and S_h is a phase-change enthalpy source term defined as

$$S_h = \frac{\partial \rho \Delta H}{\partial t} + \nabla \cdot \rho \vec{V} \Delta H \qquad (10)$$

In the enthalpy formulation, the enthalpy function, h, is the total heat content of the substance and enters the problem as a dependent variable along with the temperature. It is valid over the entire solution domain, including the solid and the liquid phases as well as the solid-liquid interface. This method is attractive in that the solution of the phase-change problem is reduced to the solution of a single equation in terms of enthalpy. There are no boundary conditions to be satisfied at the solid-liquid interface and there is no need to accurately track the phase-change boundary and to consider liquid and solid regions separately.

To account for the phase change, the governing equations have to be modified to account for the presence of both solid and liquid. The continuity equation and the momentum equation become

$$\nabla \cdot (\Theta \vec{V}) = 0 \qquad (11)$$

and

$$\Theta\frac{\partial\vec{V}}{\partial t}+\nabla\cdot(\Theta\vec{V}\vec{V})=-\frac{\Theta}{\rho}\nabla p+\frac{\Theta}{\rho}\nabla\cdot\tau+\Theta\vec{g}+\Theta\vec{F}_b+\vec{S}_v \tag{12}$$

respectively where Θ is defined as the volume fraction of fluid inside a computational cell. A unit value of Θ corresponds to a cell full of fluid whereas a zero value of Θ indicates that the cell contains all solid or obstacle. When Θ takes on a value between 0 and 1, a cell has both a fluid (liquid) and an obstacle (solid) present. The VOF transport equation is changed to

$$\frac{\partial}{\partial t}(\Theta F)+\nabla\cdot(\Theta F\vec{V})=0 \tag{13}$$

The source term takes the following form,

$$\vec{S}_v=-A\vec{V},$$

where $$A=\frac{-C(1-\Theta)^2}{(\Theta^3+\varepsilon)},$$

is used to modify the momentum equation in the mushy-region, where the fluid is modeled as flowing through a porous media. The value of C will depend on the morphology of the porous media and ε is a small number used to avoid division by zero. When a computational cell is in the liquid phase, the source term has no effect (i.e., it has a zero value). But, as the cell changes its phase, the source term grows and dominates over the transient, convective, and diffusive components of the momentum equation.

The code incorporating the features described above has been employed in previous studies. Tong [43] conducted a study on the hydrodynamics and heat transfer of a circular jet impinging onto a substrate. The study was followed by a similar study

[44] incorporating phase change at the substrate. Tong and Holt [25] performed a single molten droplet impingement study using the model described above. The aforementioned studies exhibited good agreement with results published in available literature, verifying the efficacy of the numerical code. With the validity of the numerical code established, the problem of multiple droplet impingement will now be addressed.

CHAPTER 3

PROBLEM SETUP

3.1 Grid Sizing and Convergence

The grid is the region of interest within the confines of which all simulations are carried out and pertinent data is recorded. The grid is specified so as to be able to encompass the entire impingement process from the initial state to the steady state, and possess sufficient resolution to adequately capture the phenomena being studied; its optimization however, is critical to avoid unnecessary wastage of computer resources. A grid consists of cells in the x and y directions, spaced either uniformly or non-uniformly. A uniform grid is one in which the cell spacing remains the same throughout the grid. A non-uniform grid may have cell spacing varying from cell to cell. Non-uniform grids are used when the most prominent activity takes place in a localized region in the grid. The grid density is increased in the vicinity of the region with most activity and reduced elsewhere in the grid. This enables judicious utilization of computer resources; however, care needs to be taken to ensure the aspect ratio of the cells (ratio of width in the x-direction to that in the y-direction), is not too large or too small. To determine an optimum spacing, a grid sensitivity study is conducted. For the purpose of this study, a grid spacing of 0.03 mm, 0.01 mm and 0.0075 mm is used. A simulation of two droplets impinging onto a substrate is performed. The results are presented in Figure 3.1 and Figure 3.2.

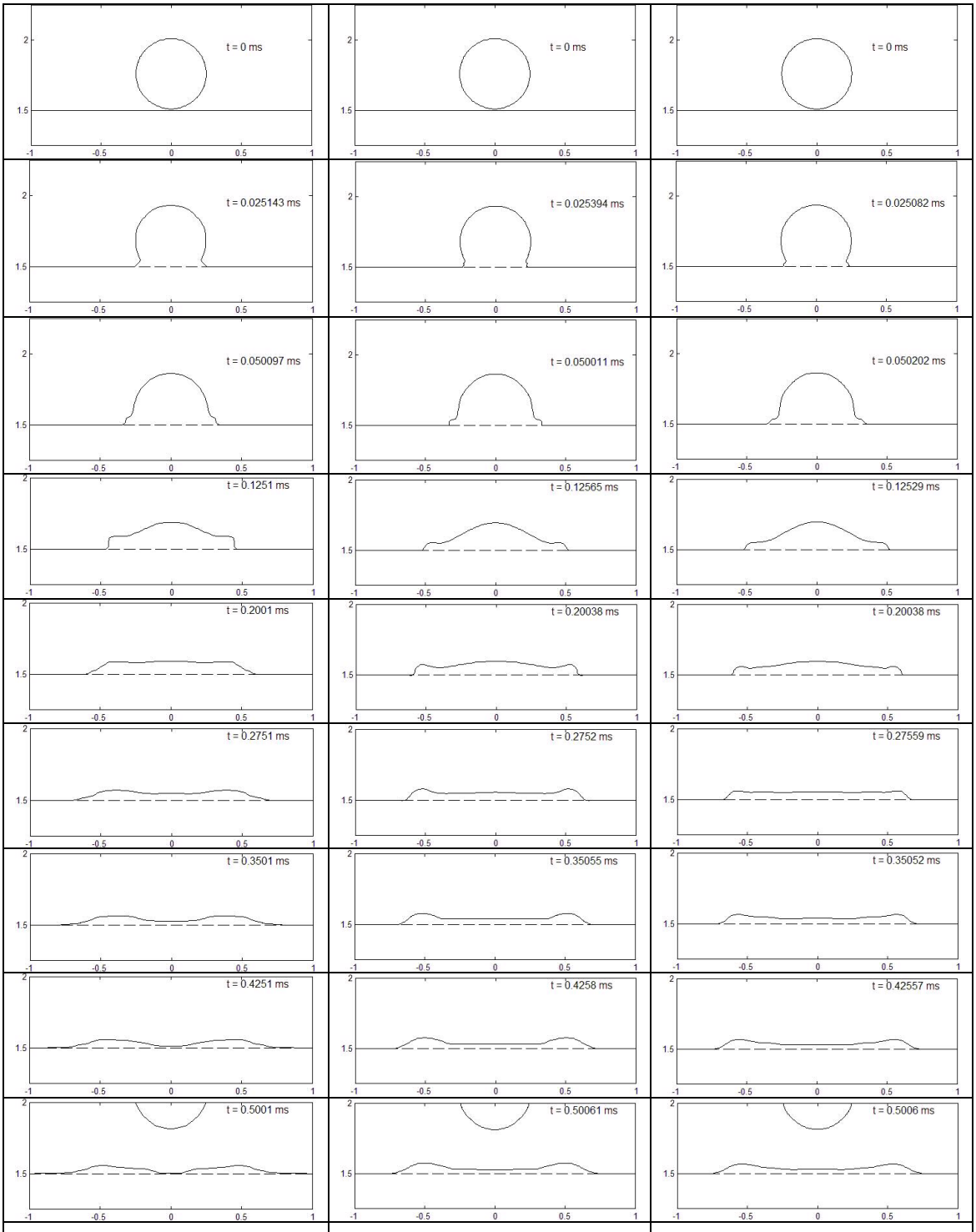

Figure 3.1 Grid sensitivity study (I) 0.03mm, (II) 0.01mm and (III) 0.0075mm

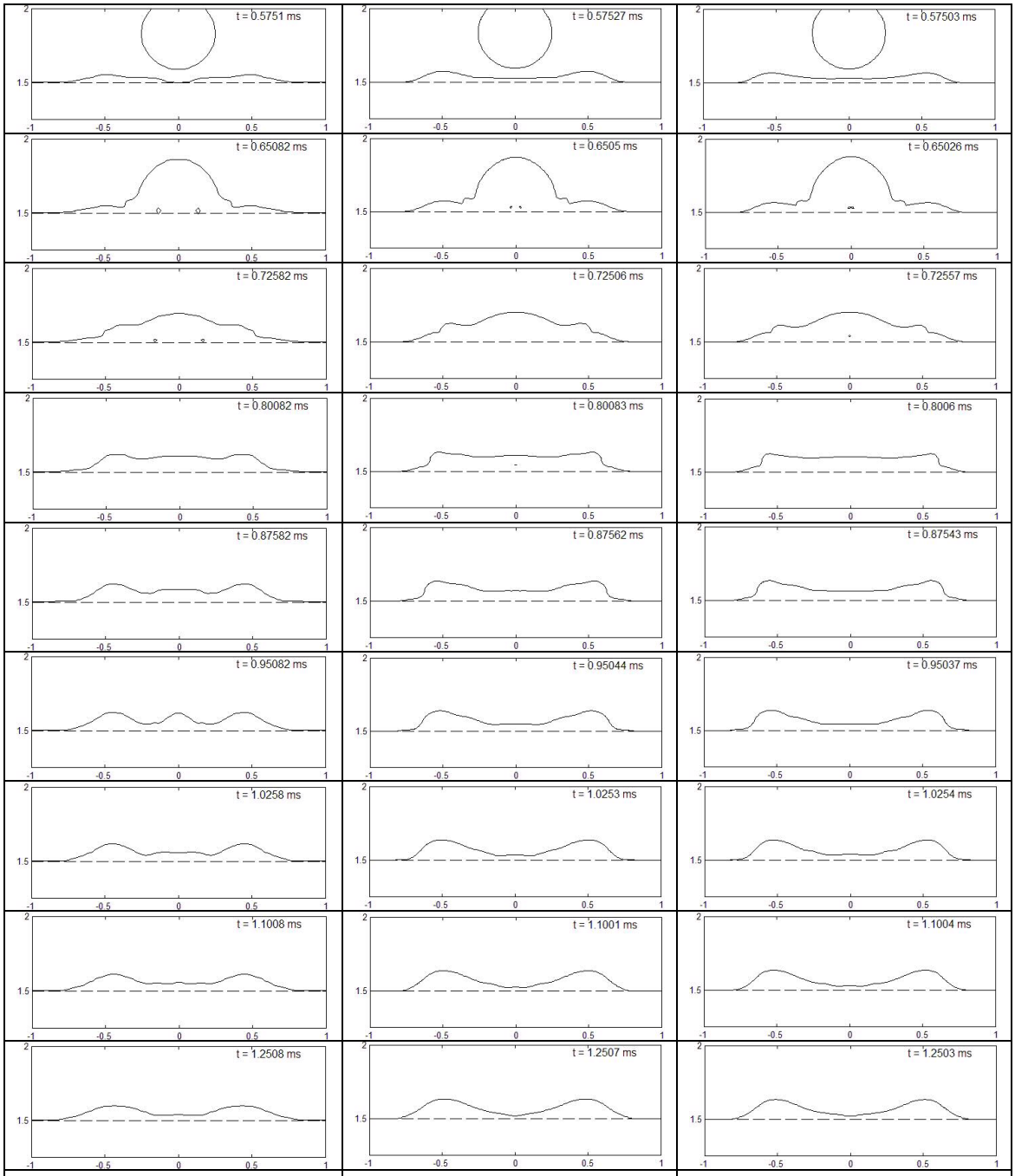

0.03 mm	0.01 mm	0.0075 mm

Figure 3.2 Comparison of results with grid refinement

The objective of the grid sensitivity study is to refine the grid until convergence is obtained. Convergence is a characteristic feature that underlines the accuracy of a

numerical simulation. It is of essence to know that the simulation being conducted is true to the extent that the numerical model is capable of. This is tested by refining the grid so that successive refinements do not reveal any significant deviation in results obtained. From Figures 3.1 and 3.2, it can be seen that there is a significant departure in the shape of the free surface from I to II. However this departure is minimal from II to III. Thus, the grid sensitivity study reveals that a grid spacing of 0.01 mm is sufficient to accurately model the given problem.

The factors which determine the extent of the grid in the current problem are the diameter of the droplet and the width and depth of the substrate. The width of the substrate is chosen so as to ensure that the droplet spread remains within the grid and does not flow out of the boundary of the grid. The substrate depth is chosen to be able to capture the remelt depth and temperature variations due to heat transfer. The grid for the standard case, i.e. the case against which all other parametric studies are compared with, is shown in Figure 3.3.

In the present study, a numerical investigation of the impingement and solidification behavior of two molten tin droplets is being conducted. The entire impingement process can be assumed as axisymmetric since the droplets are spherical and have the same vertical trajectory, i.e. they impact the substrate along an axis orthogonal to the substrate. The study of an axisymmetric slice enables considerable optimization of computer resources. The overall behavior may be obtained by revolving the slice through 360º.

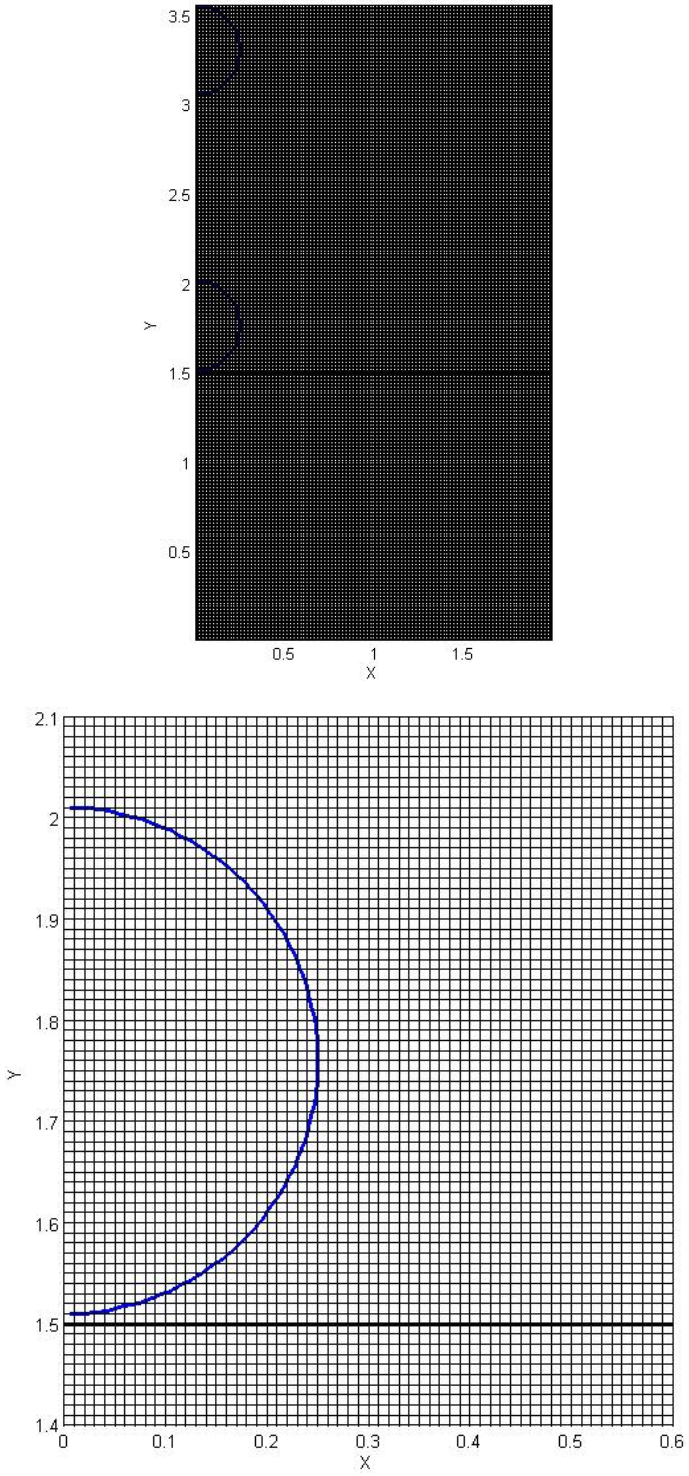

Figure 3.3 Complete grid (top) and a magnified view of the grid (bottom)

3.2 Boundary Conditions

The conditions at the boundaries of the grid need to be specified for the problem being studied. Since the grid is rectangular, there are four boundary conditions which need to be applied, one at each face of the grid. A rigid free-slip condition is applied to the top and left boundaries. A rigid no-slip condition is applied to the bottom boundary. A continuative outflow condition is prescribed for the right boundary. In addition to these conditions, an adiabatic boundary condition is applied on all free surfaces. A schematic view of the initial free surface shapes and the boundary conditions is shown in Figure 3.4.

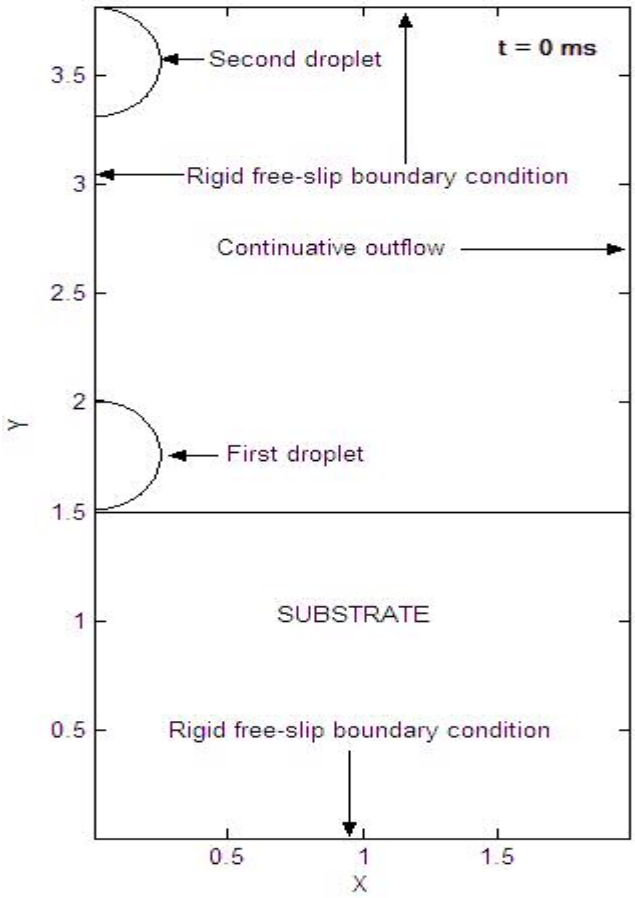

Figure 3.4 Initial state and boundary conditions

3.3 The Input File

The factors that need to be taken into account for determining the grid have been described. The appropriate boundary conditions that are to be applied have also been outlined. These conditions and values for all other variables must be furnished to the flow-solver via an input file. Information about the problem geometry, initial conditions, fluid parameters, thermal parameters and numerical parameters are fed to te flow-solver with input variables grouped into format-free namelists. Each namelist contains a set of input variables that control related functions in the problem setup. The more significant namelists and their variables are described below. It is to be noted that all variables pertaining to time, length, mass and temperature are in units corresponding to ms, mm, mg and K respectively. Details can be obtained from [10,35].

3.3.1 Numerical Parameters

Input variables controlling the numerical algorithms reside in the namelist called NUMPARAM. The notable parameters in this list are DELT, DTMAX, KB, KT, KL, KR, and PLTDT. Their meaning and values used in the code are listed below.

Table 3.1 Numerical Parameters

Variable name	Description	Value used
DELT	Initial time step of calculation	1.0e-5
DTMAX	Maximum allowed timestep	1.0e-3
PLTDT	Time increment between generation of data files	2.5e-2
KB	Boundary condition flag for the bottom boundary	2
KT	Boundary condition flag for the top boundary	1
KL	Boundary condition flag for the left boundary	1
KR	Boundary condition flag for the right boundary	3

3.3.2 Fluid Parameters

Fluid properties are controlled by variables listed in the FLDPARAM namelist. Quantities such as surface tension, kinematic viscosity, density, acceleration due to gravity and initial velocity are defined here. The variable names used and their descriptions are listed in the table below.

Table 3.2 Fluid Parameters

Variable name	Description
SIGMA	Coefficient of surface tension
RHOF	Fluid density
XNU	Coefficient of kinematic viscosity
GY	Acceleration due to gravity in positive y direction
VI	Initial fluid velocity in positive y direction

3.3.3 Thermal Parameters

Thermal properties are controlled by variables listed in the HEATEQ namelist. Quantities such as initial droplet and substrate temperature, specific heat, and latent heat are specified in this list. The variable names used and their description are listed in the table below.

Table 3.3 Thermal Parameters

Variable name	Description
TID	Initial temperature of the droplet
TIP	Initial temperature of the substrate
CPD	Specific heat capacity of the droplet
LHPC	Latent heat of phase change

3.3.4 The Standard Case

A simulation of the problem being studied is first carried out using parameters obtained from published literature [29]. This case is referred to as the standard case. This case is also used as a reference to compare results from parametric studies. The grid size and fluid and thermal properties used in the standard case are tabulated below. A guide to performing the simulation is presented in Appendix A. The input file for the standard case is listed in Appendix B.

Table 3.4 Specifications of the Standard Case

Parameter	Value (SI units)
Substrate width	0.004 m
Substrate depth	0.0015 m
Grid dimensions ($x \times y$)	200 × 382
Cell spacing	0.00001 m
Droplet diameter	0.0005 m
Initial droplet velocity	3 m/s
Droplet density	7000 kg/m^3
Surface tension coefficient	0.621 N/m
Kinematic viscosity	3.9e-7 m^2/s
Initial droplet temperature	600 K
Initial substrate temperature	303 K
Droplet thermal conductivity	30 W/m-K
Substrate thermal conductivity	63.9 W/m-K
Specific heat capacity	250 J/kg-K
Latent heat of phase change	59500 J/kg
Melting point of tin	507.5 K

CHAPTER 4

RESULTS

4.1 Standard Case Simulation

The standard case has been described in the previous chapter. The simulation of the standard case is carried out and the results are obtained. Figure 4.1 presents the impact and solidification of two molten tin droplets proceeding in time. The contour marked in red represents the melting or solidification front, depending whether the front is progressing or receding in the substrate. The droplet is completely solidified when the red contour (which represents a temperature of 507.5 K) disappears. As can be seen from the figure, the first droplet solidifies at 0.49721 ms and the second droplet solidifies at 1.1565 ms. It is also observed that the solidification process begins the moment the first droplet impacts the substrate. Therefore, it can be inferred that the time-scale for the solidification process is comparable to the time-scale for the spreading process. As the droplet spreads, the temperature of the leading (or outer) edge of the droplet is found to be much lower than the temperature at the centre of the splat. Hence, the solidification of the splat is predicted to begin at the leading edge and then progress towards the central region of the splat. This also implies that the onset on solidification impedes the spreading of the droplet. These results are in agreement with those obtained in [3,15]. However, for the second droplet, although the temperature of the leading edge is still lower in comparison to the central region of the second splat,

the process of solidification progresses towards the free surface and the termination of the solidification front is found to occur at either the central region or the crown (the highest point of the solidified splat).

The temperature contours in the droplet-substrate region at times t = 0.10064 ms and t = 0.6252 ms are shown in Figure 4.2. The curve corresponding to 507.5 K is the melting front and the curve corresponding to 304 K (which is 1 K higher than the initial temperature of the substrate) signifies the heat-affected region in the substrate. At t = 0.10064 ms the first droplet has already impacted the substrate and the melting front is advancing into the substrate. At t = 0.6252 ms the second droplet has already impacted the solidified splat and the state represents the advancement of the melting front through the previously solidified splat. Contrary to assumptions made by previous researchers, the overall heat transfer is not one-dimensional. The temperature field in the substrate is observed to exhibit two-dimensional features, as can be inferred from Figure 4.2. Conduction is found to be more axial in the vicinity of the axis of symmetry, and increasingly radial at the leading edge of the spreading droplet. Therefore, the assumption of one-dimensional heat transfer may be valid only at central regions of the substrate. This nature of heat conduction is obtained during the spreading and solidification of both the first and second droplets. These results are in agreement with those obtained by Zhao et al. [3] for a single droplet and by Kang et al. [18] for two droplet impingement.

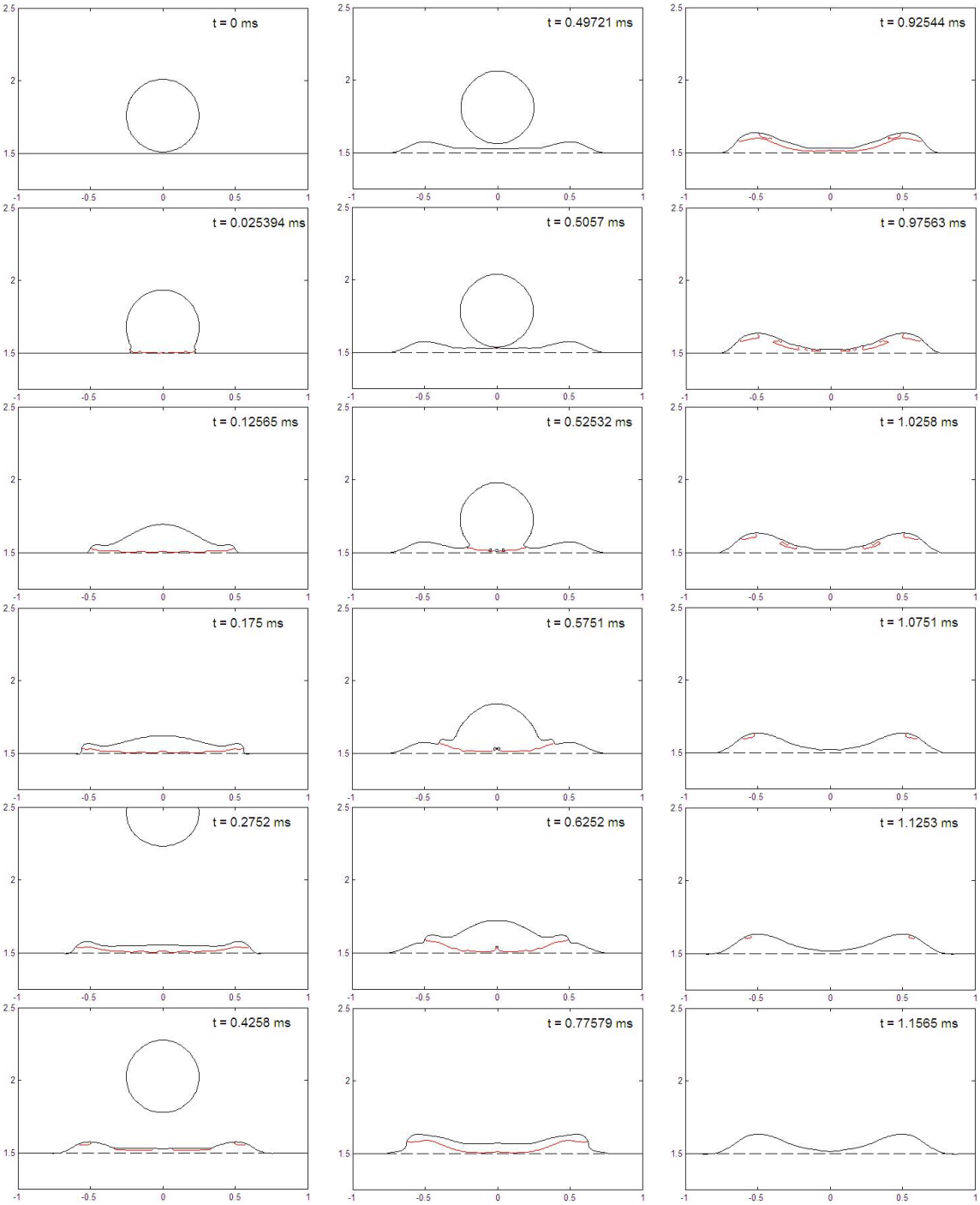

Figure 4.1 Chronological progression of sequential impact of two molten droplets

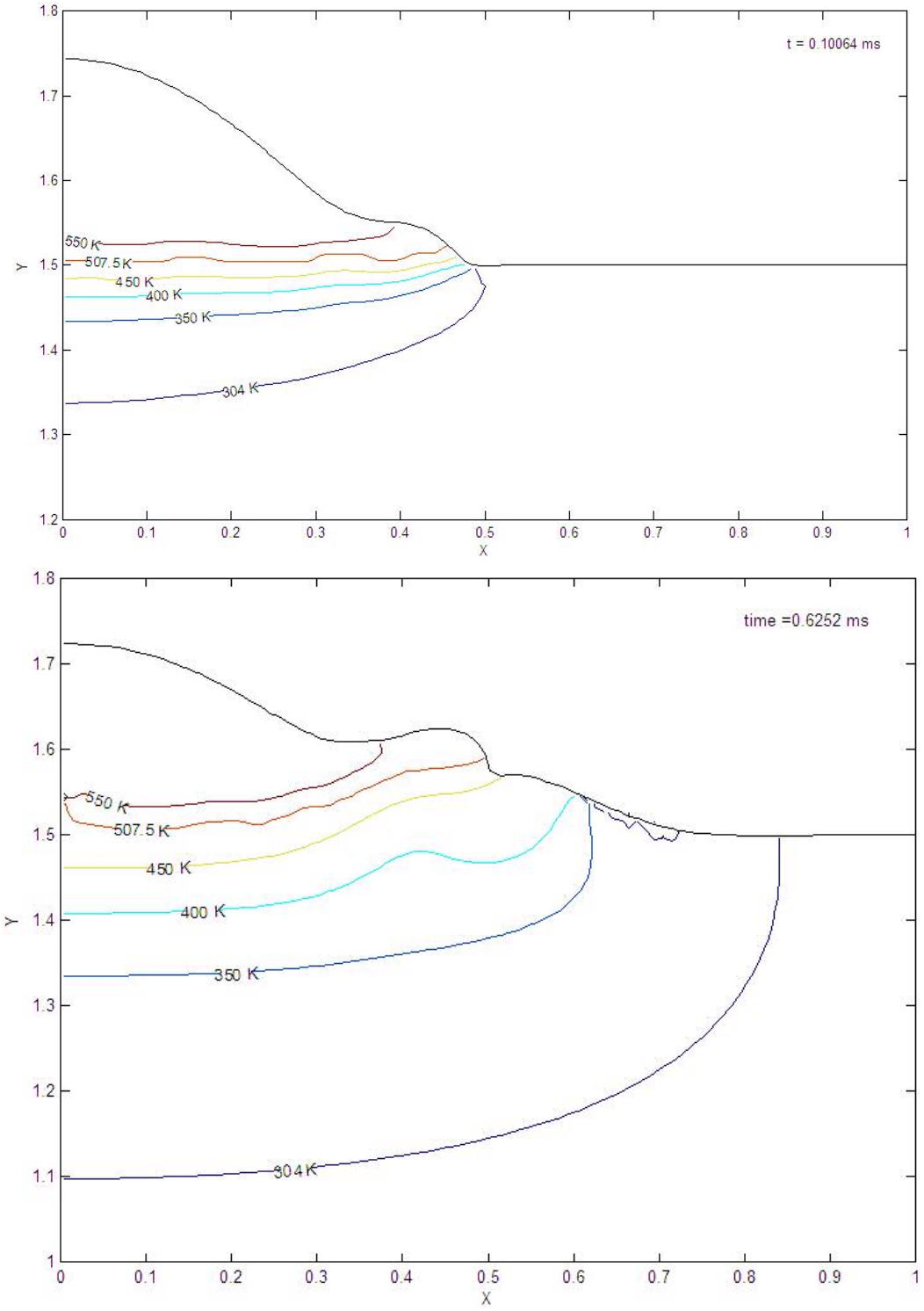

Figure 4.2 Temperature contours at t = 0.10064 ms (top) and t = 0.6252 ms (bottom)

4.2 Parametric Studies

The role of initial droplet and substrate temperatures in achieving a uniform splat, with controlled amounts of substrate remelting has only been highlighted thus far. It is desired to quantify the effects of these variables by introducing dimensionless parameters that are indicative of the spreading, solidification and remelting behavior. Two parameters of significance known as the spread factor and the Stefan number are defined as follows.

The spread factor, ξ, is representative of the extent to which the droplet spreads after impact with the substrate. It is defined as the ratio of the diameter of the splat to the initial diameter of the droplet.

$$\xi = \frac{Splat\ Diameter}{Initial\ Droplet\ Diameter} = \frac{D}{D_0}$$

The Stefan number is a non-dimensional number and is defined as the ratio of the quantity of heat required to raise the temperature of the substrate to its melting point, to the latent heat of fusion.

$$Ste = \frac{Sensible\ Heat}{Latent\ Heat} = \frac{C_p(T_m - T_p)}{L}$$

where C_p is the specific heat capacity, L is the latent heat of phase change, and T_m and T_p are the melting point and initial temperature of the substrate respectively.

Before the results are discussed, the definitions of solidification time and maximum remelt depth are stated for clarity and completeness. The solidification time is defined as the time taken for the temperature of the entire droplet to fall below the melting point of the material of the droplet, after the droplet has impacted the substrate.

The first droplet is situated in such a way that it impacts the substrate at the instant the simulation begins. Thus for the first droplet, the solidification time is recorded from the time instant t = 0 ms, until the entire splat has completely solidified. The second droplet is situated at a height above the substrate such that its impact with the first droplet occurs only after the first droplet has completely solidified. This is done to preserve the independence of the behavior of the first droplet from the second droplet, thereby allowing for the accurate determination of the solidification time of the first droplet. Since the first droplet has completely solidified before the impingement of the second droplet, the solidification time for the second droplet is recorded from the instant it impacts the first splat, until the second droplet has completely solidified. The time elapsed during the fall of the second droplet is not factored into the solidification time.

The maximum remelt depth R, is defined as the depth below the surface of the initial substrate up to which the melting front penetrates on impact with the substrate. The melting front corresponds to the location of the contour whose temperature is equal to the melting point of the material of the droplet selected; in this case, 507.5 K.

4.2.1 Effect of Initial Droplet Temperature, T_d

The effect of initial droplet temperature on the spread factor, solidification time and remelting depth is studied. Droplet temperatures are varied as 550 K, 650 K, 750 K and 850 K, and results are compared with the standard case. In Figure 4.3, only the free surfaces corresponding to initial droplet temperatures of 600 K (standard case), 750 K and 850 K are shown. As can be seen from Figure 4.3, a higher initial temperature of the droplet translates into an increase in spread factor. The depth of the central location

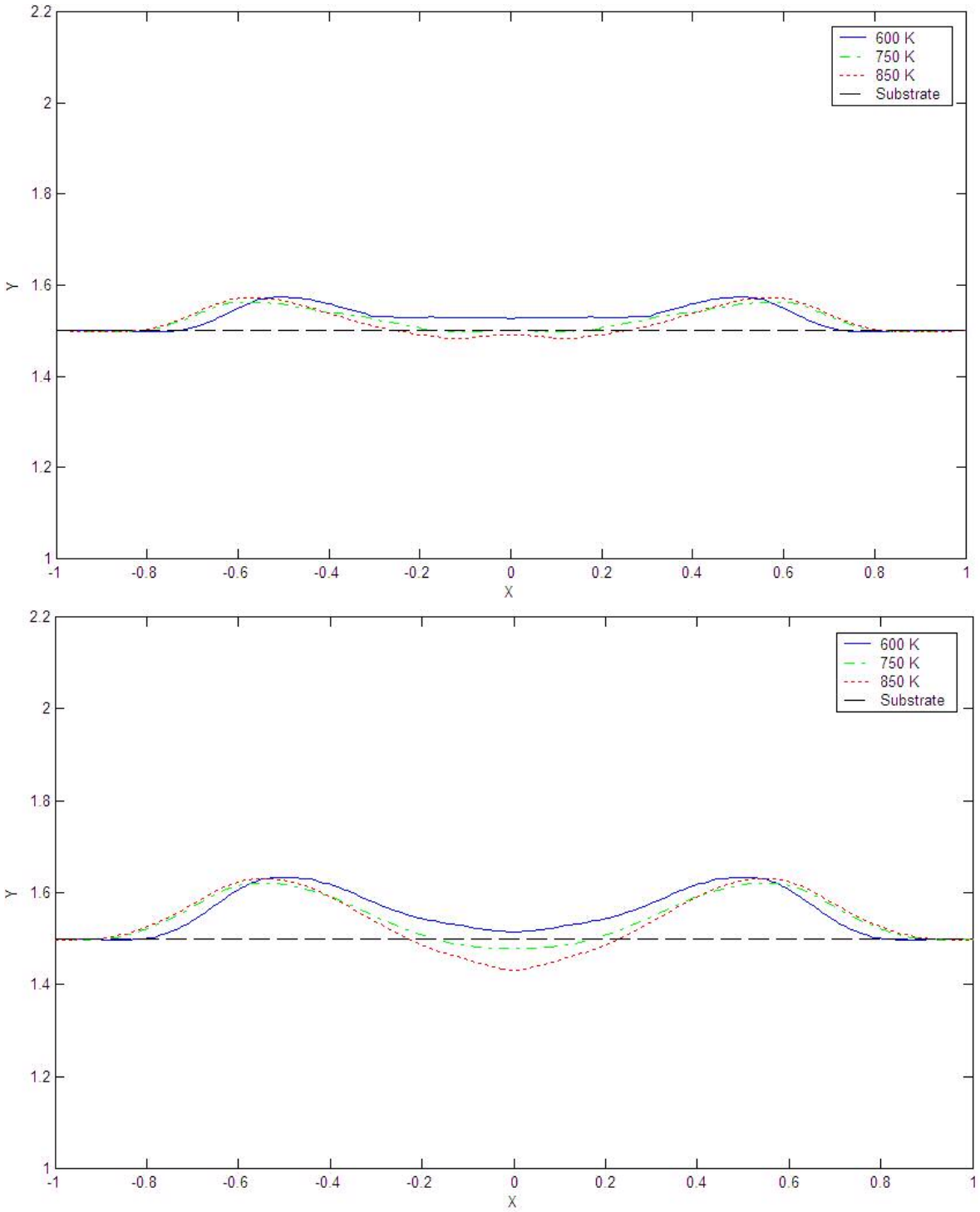

Figure 4.3 Effect of initial droplet temperature on free surfaces of solidified splats: 1st droplet (top) & 2nd droplet (bottom)

of the splat also increases, and for the cases of 750 K and 850 K, the location of the centre of the final solidified splat (after impact of second droplet), is found to be lower than the level of the initial substrate. It can be deduced that a portion of the substrate was remelted, displaced in the radial direction and then solidified. This pit formation is a result of excessive remelting, and is undesired from a manufacturing stand point.

Figure 4.4 highlights the variation of solidification times of the first and second droplet with increase in initial droplet temperature, T_d. It can be seen that, in general, the time taken by either droplet to solidify is higher as T_d is increased. Another point of significance is that the second droplet takes longer to solidify than the first droplet. A droplet with a higher initial temperature possesses a larger value of superheat. The droplet on impact with the substrate, therefore, has a greater amount of heat energy to transfer to the substrate. Consequently, the time taken to transfer the heat energy to the substrate is longer. Since the process of solidification can begin only after all the superheat is removed from the droplet, the time taken for solidification is greater when T_d is increased. From Figure 4.4, it is evident that the second droplet takes longer than the first droplet to solidify. As first droplet has just solidified before the second droplet impacts it, the temperature at the surface of the solidified first splat is close to the melting point. Therefore, the second-droplet-first-splat interface has a lower temperature gradient when compared to the gradient experienced by the first droplet when it impacts the cold substrate. This results in a lower rate of heat transfer, and therefore the second droplet takes longer to solidify than the first droplet.

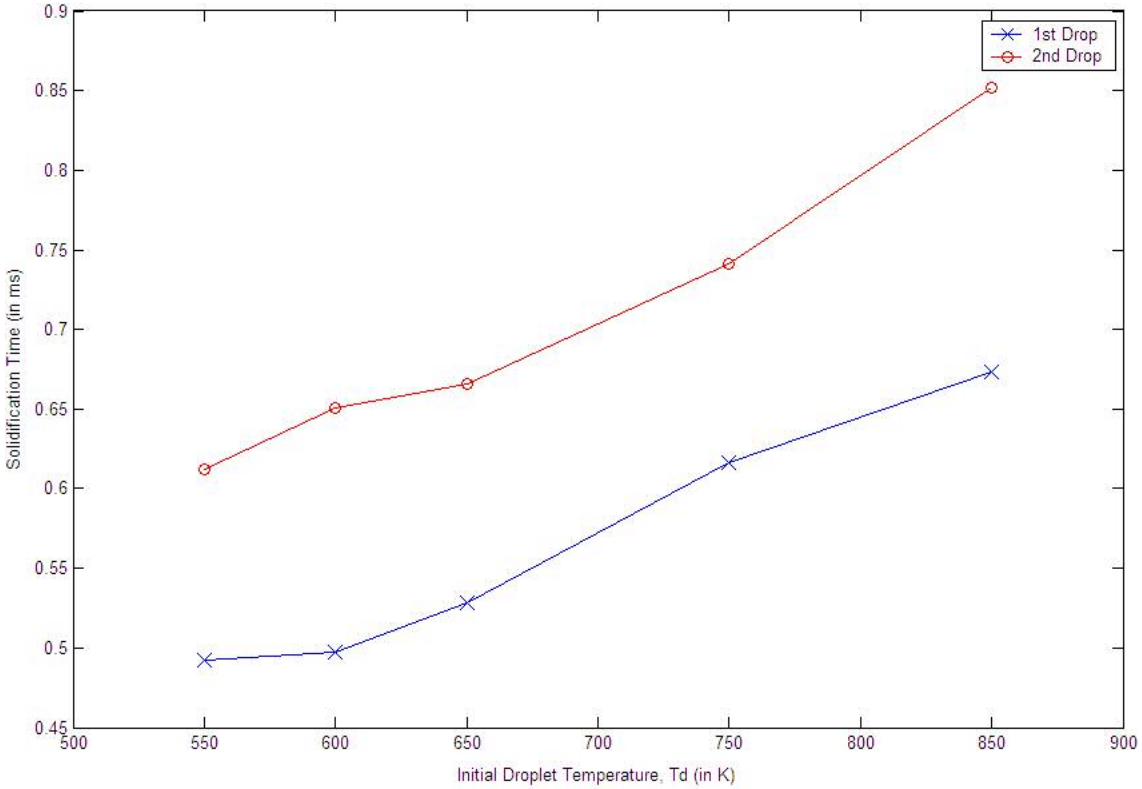

Figure 4.4 Variation of solidification times of first and second droplets

The influence of T_d on the maximum spread factor ξ, of the first and second droplets is obvious from Figure 4.5. The initial droplet temperature is normalized and is called the superheat parameter, SHP, where,

$$SHP = \frac{T_d - T_m}{T_m - T_p}$$

It can be inferred from the plot of ξ vs SHP that ξ, and hence the maximum diameter of the splat, increases as the initial droplet temperature is increased. The high thermal energy associated with a higher temperature results in a longer solidification time (as observed earlier) during which the motion of the droplet on the surface takes place unrestricted by the solidification front. This results in a larger value for ξ.

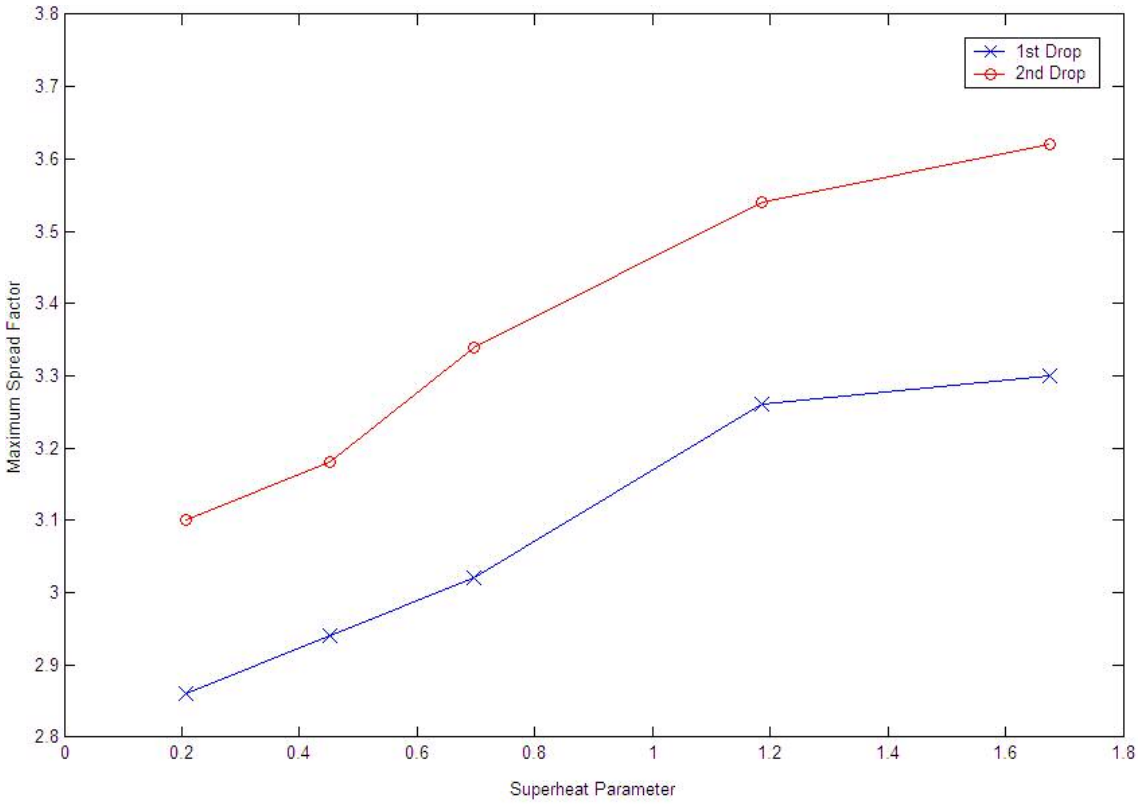

Figure 4.5 Variation of spread factor with superheat parameter

The influence of T_d on the maximum depth of remelting, R, is illustrated in Figure 4.6. R is found to increase almost linearly with increase in T_d, for the parameters used in this study. The increase in R is attributed to the increase in thermal energy associated with higher values of T_d, which is utilized to melt the substrate as the droplet impacts the substrate. It can also be observed that remelting of the substrate by the first droplet does not occur for temperatures $T_d < 600$ K, since the droplet does not possess enough heat energy to melt the substrate during impact and spreading. The heat energy transferred to the substrate is insufficient to raise the temperature of the substrate to its melting temperature. The threshold temperature T_d for the second droplet to cause remelting on impact is found to be same as for the first. However, the value of R for the

second droplet is observed to be greater than the first droplet. This is easily inferred since the second-droplet-first-splat interface is at a higher temperature than the first-droplet-substrate interface. Hence, a lesser amount of heat energy is required to melt the first splat and a greater amount of heat energy is left to cause remelting.

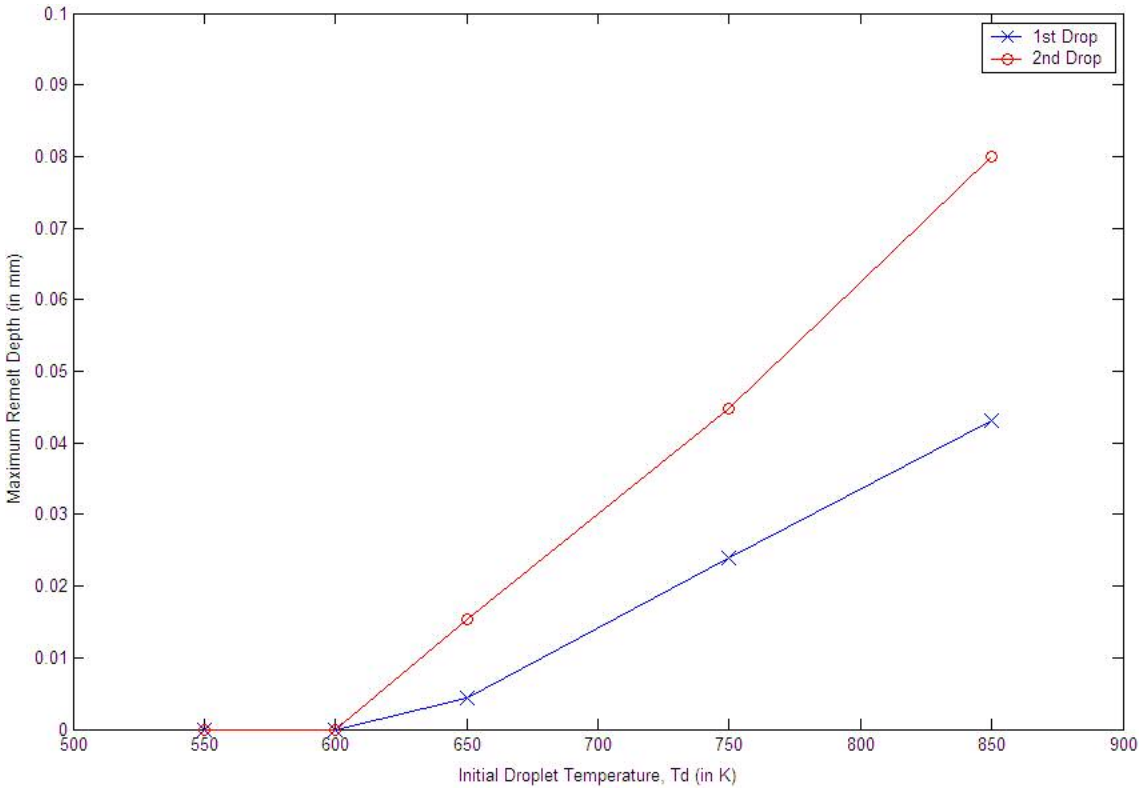

Figure 4.6 Variation of maximum remelt depth with initial droplet temperature

4.2.2 Effect of Initial Substrate Temperature, T_p

The effect of initial substrate temperature on the spread factor, solidification time and remelting depth is studied. Simulations are carried out for substrate temperatures of 350 K and 400 K and compared with the standard case. Figure 4.7 depicts the free surfaces corresponding to initial substrate temperatures of 303 K, 350 K and 400 K. The spread factor is observed to increase as the initial substrate temperature

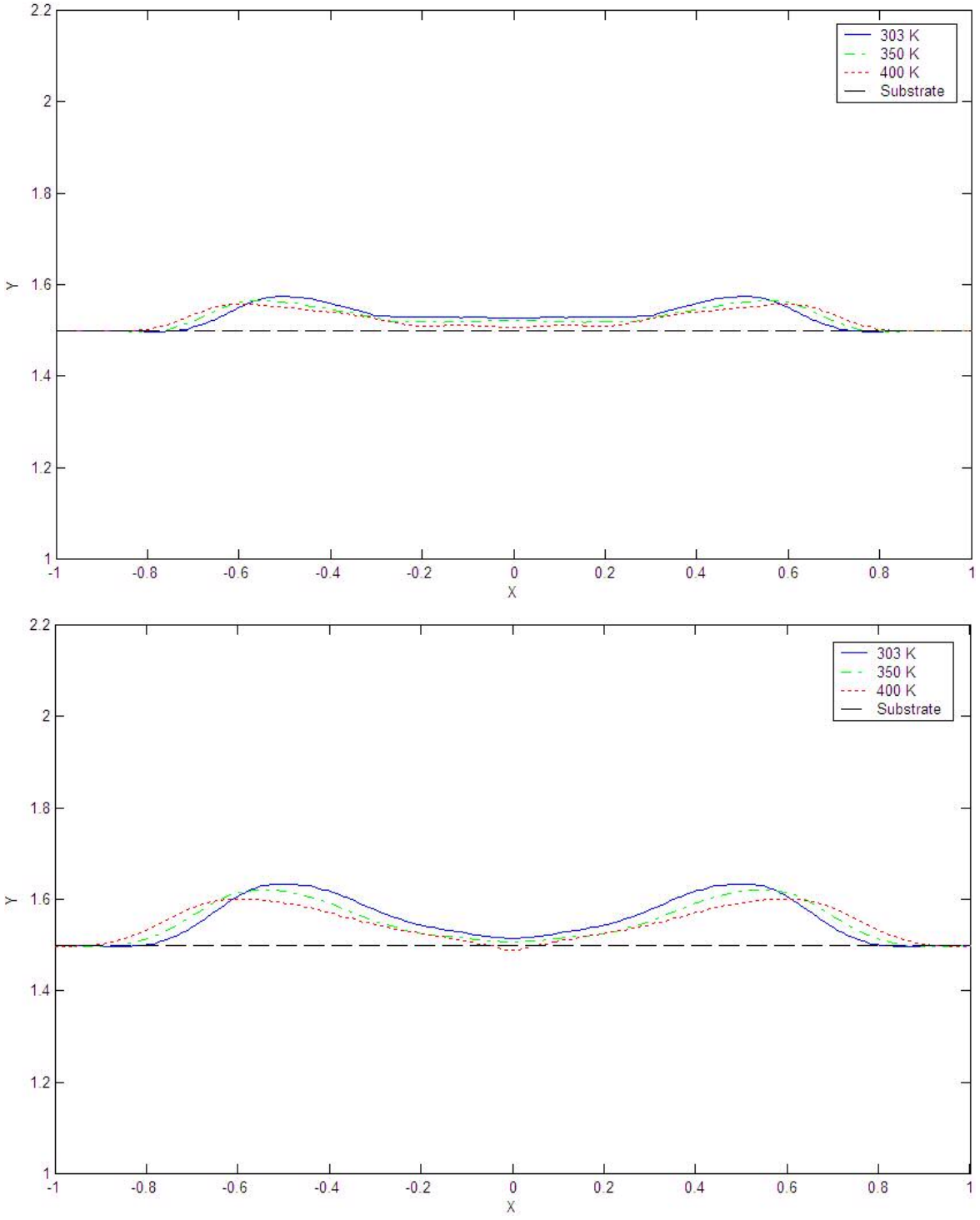

Figure 4.7 Effect of initial substrate temperature on free surfaces of solidified splats: 1st droplet (top) & 2nd droplet (bottom)

T_p, is increased. The depth of the central location of the splat also increases. For the case where T_p = 400 K, the final height of the central region of the splat after the second droplet has completely solidified is found to be lower than the initial height of the substrate. It is obvious that a small amount of substrate material must have been remelted and deposited in the radial direction before solidifying. It is also noted that the droplets spread more smoothly over the substrate as T_p is increased, as is inferred from the decreasing heights of the solidified splats.

Figure 4.8 illustrates the variation of solidification times of the first and second droplet with increase in T_p. Along similar lines as previously observed in the case of the effect of initial droplet temperature, the solidification time increases as the substrate temperature is increased, and the second droplet takes longer to solidify than the first droplet. This behavior can be explained in the light of the fact that the substrate at a relatively higher temperature presents a smaller gradient for heat transfer, which results in a lower rate of heat transfer. Droplets impacting a substrate with higher values of T_p therefore, take longer to solidify. The second droplet impacts the splat of the first droplet a short while after it has solidified and thus has only a nominal gradient available for heat transfer. This gradient is less than that available for the first droplet since the substrate temperature is lower than the surface temperature of the solidified first splat. The rate of solidification for the second droplet is lower than the first droplet, and hence it takes longer to solidify.

The influence of T_p on ξ, of the first and second droplets can be seen from Figure 4.9. The characteristic number used in this case is the Stefan number. As the

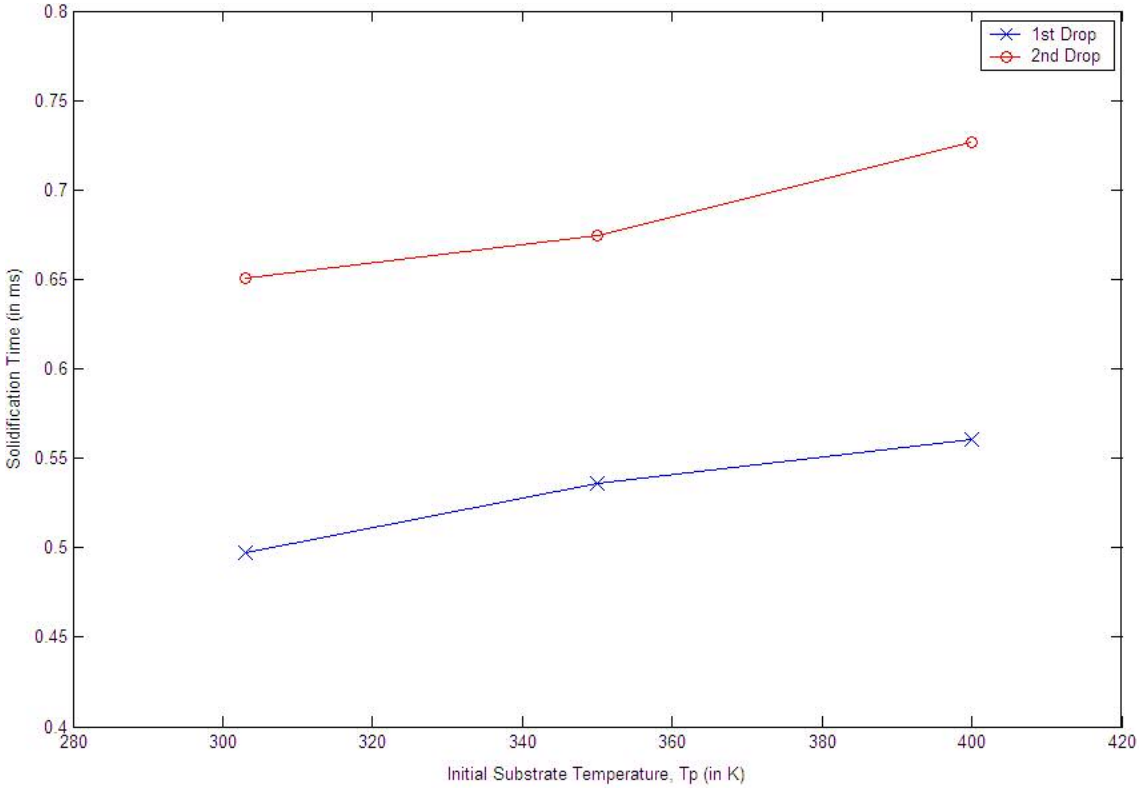

Figure 4.8 Variation of solidification times of first and second droplets

Stefan number increases (which implies that the initial substrate temperature decreases), ξ decreases. A lower value of Stefan number is associated with a higher value of T_p. Due to the lower temperature gradients involved, the majority of the droplet remains in molten state for a longer period, which promotes the overall flow, and results in an increase in the value of ξ.

The influence of T_p on the maximum depth of remelting, R, is illustrated in Figure 4.10. No remelting of the substrate due to the first droplet occurs for $T_p = 303$ K (Ste = 0.859). The combination of initial substrate and droplet temperatures for the standard case is found to be insufficient to enable the first droplet to cause remelting. For $T_P > 303$ K, a small amount of remelting is observed. The second droplet however,

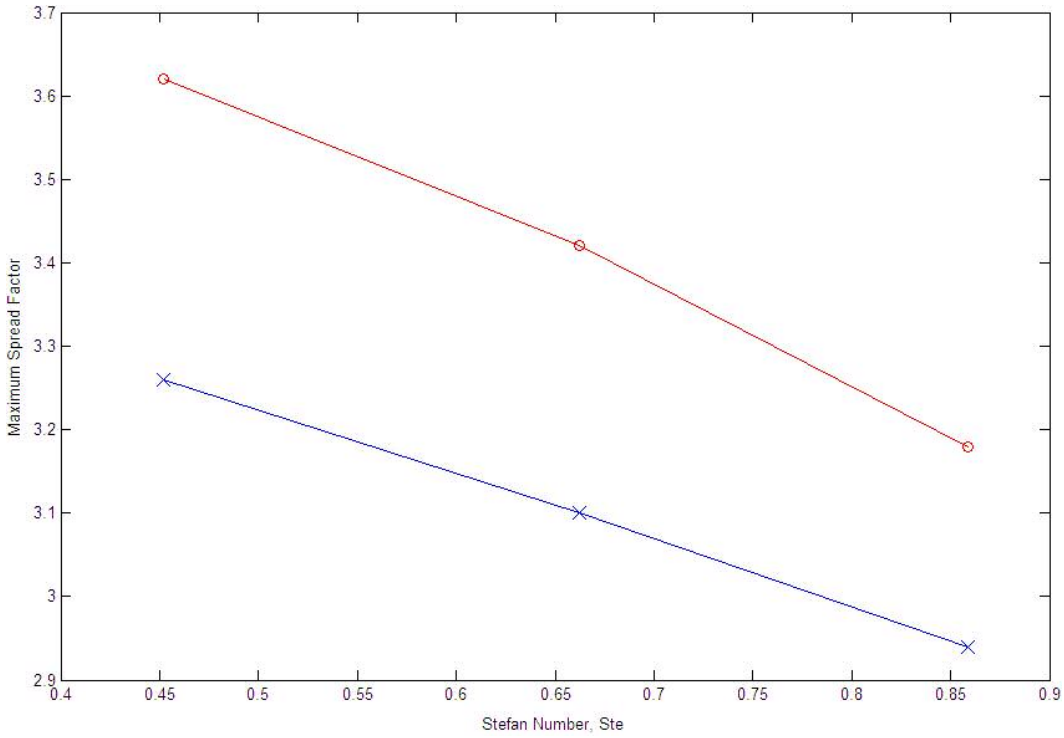

Figure 4.9 Variation of maximum spread factor with Stefan number

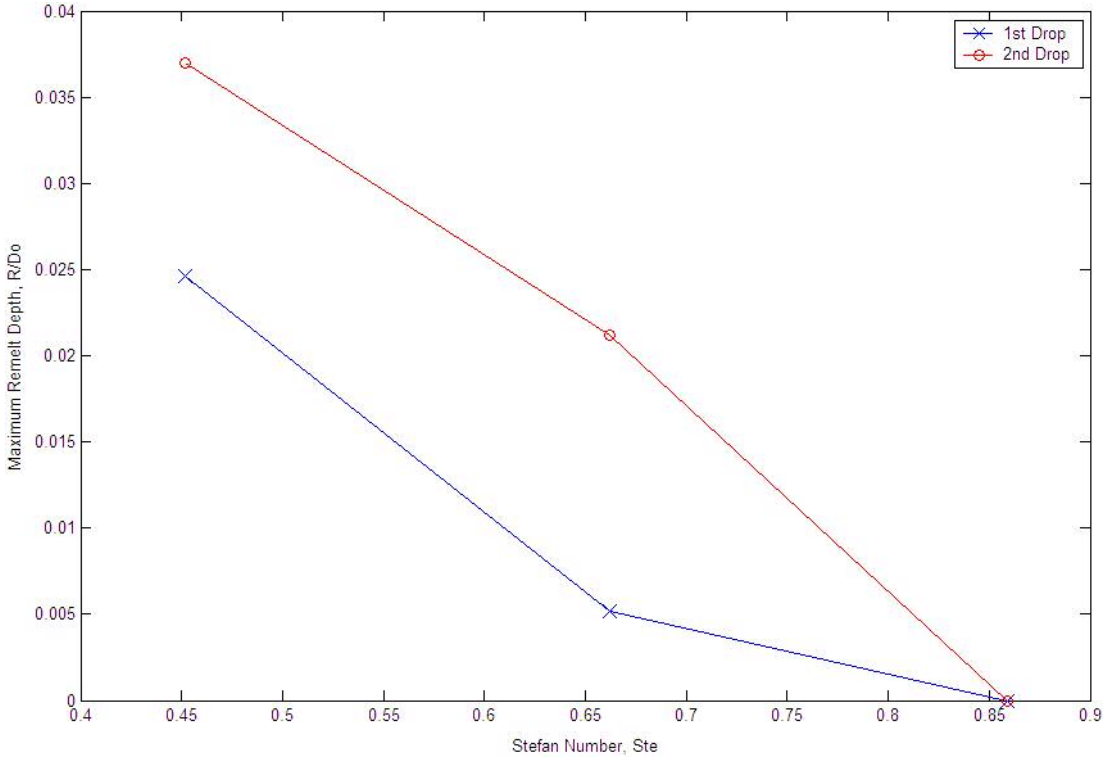

Figure 4.10 Variation of maximum remelt depth with Stefan number

achieved a greater amount of remelting since the impact of the second droplet takes place soon after the first droplet solidifies. The second-droplet-first-splat interface is nearly at the melting point of the material, and hence, only a small amount of heat energy is required to bring the splat to the melting temperature. The remaining heat transfer serves to advance the melting front and therefore, an increase in R is observed.

The above observations reveal the role the initial substrate temperature plays in the spreading, solidification and remelting behavior. An increase in the value of T_p does promote substrate remelting and also results in an increase in the spread factor of the impinging droplets. From the standpoint of manufacturing, an increase in substrate temperature results in a smoother spreading of the droplet over the substrate, which is a desirable flow characteristic.

4.2.3 Effect of Latent Heat, L

The latent heat is a property of the material of the substrate and droplet. The latent heat of fusion is usually constant for a given material; however, its presence in the Stefan number, and the knowledge of the effect of Stefan number on the spread factor, demands a study into the effects of latent heat on the overall impingement and solidification phenomena.

A parametric study into the effect of latent heat on the spread factor, solidification time and remelt depth is conducted. The final splat shapes of the solidified splats of the first and second droplets are shown in Figure 4.11. For the purpose of the study, the values of latent heat are varied as 25% and 175% of the value used in the standard case. The increase in spread factor as the latent heat is increased, is very

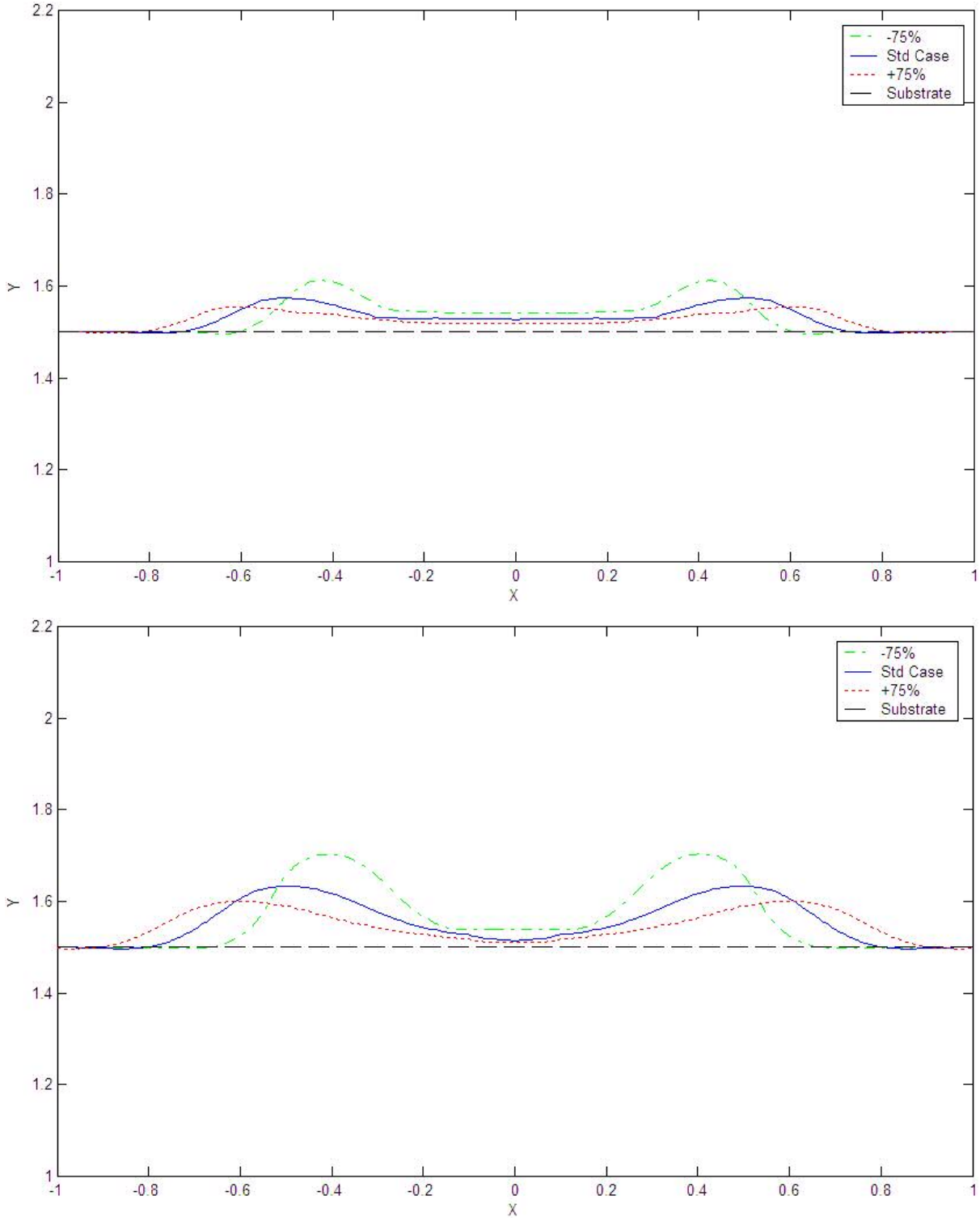

Figure 4.11 Effect of latent heat on free surfaces of solidified splats:
1st droplet (top) & 2nd droplet (bottom)

apparent. The solidification and remelting behavior can be studied after closer scrutiny.

The influence of the variation of latent heat on the time taken for the first and second droplets to solidify can be grasped from Figure 4.12. As the latent heat is increased from the standard case, the solidification times are found to increase, and vice versa. This behavior can be explained in the light of the fact that the latent heat represents the amount of heat that is absorbed or released when the droplet melts or solidifies, respectively. A greater amount of latent heat implies that there is a larger reserve of energy that has to be transferred out of the droplet before the solidification process can even begin. By the same token, a lesser amount of latent heat implies that solidification begins earlier and hence, the solidification time is shorter.

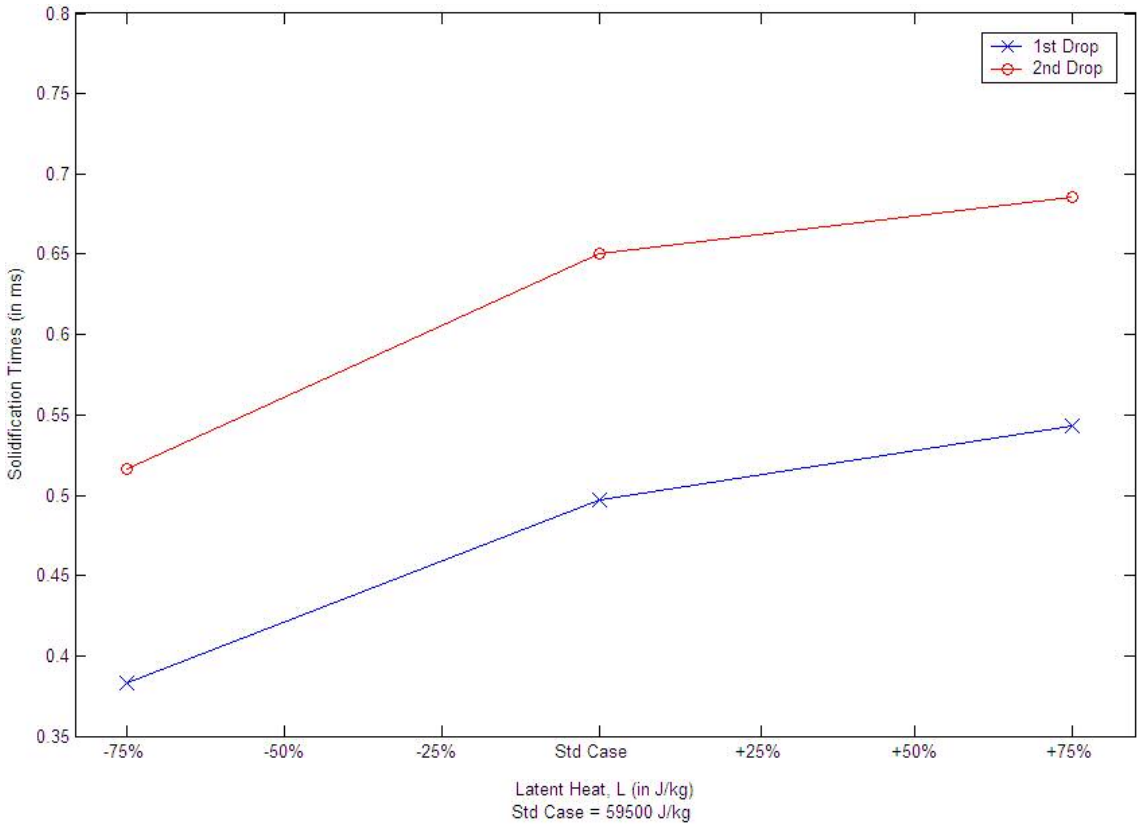

Figure 4.12 Variation of solidification times of first and second droplets

The above explanation also accounts for the behavior of the maximum spread factor ξ with variation in latent heat. Figure 4.13 illustrates the influence of the Stefan number on the value of ξ of the two molten droplets sequentially impinging onto the substrate.

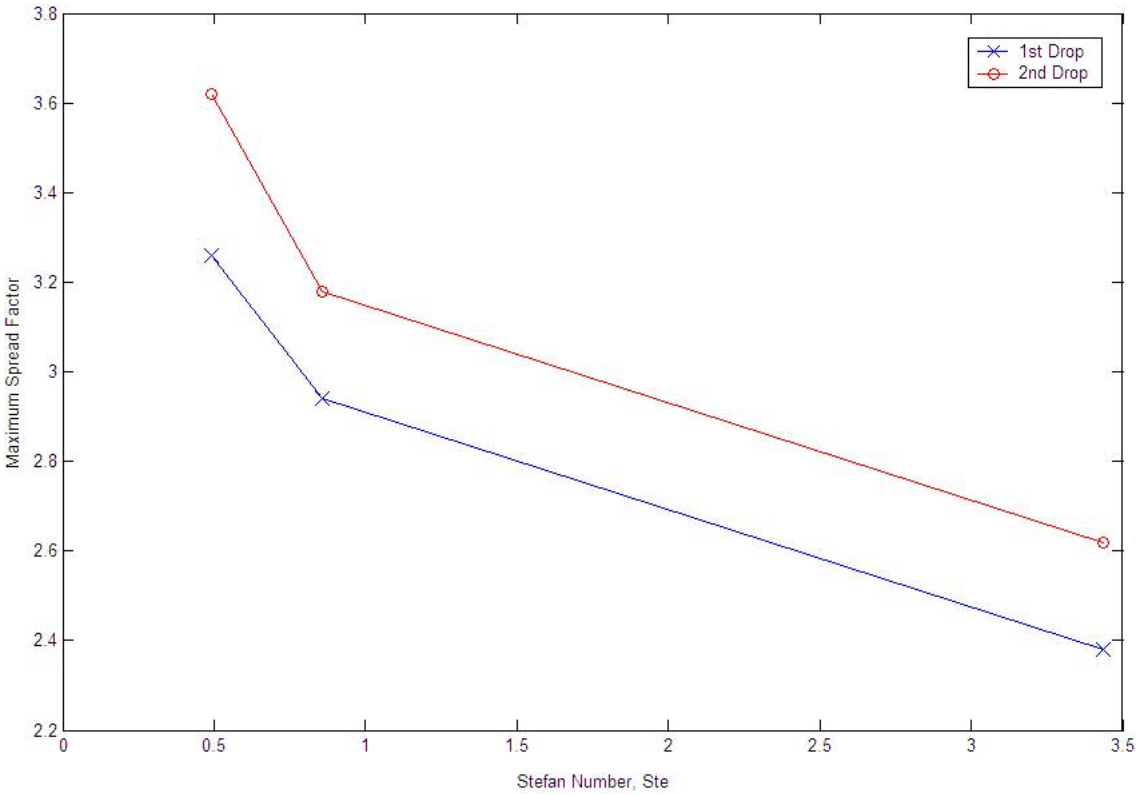

Figure 4.13 Effect of latent heat on the maximum spread factor

As the Stefan number increases (and the amount of latent heat decreases), ξ is found to decrease. Since the time for solidification is longer for lower values of the Stefan number, the droplet motion is unrestrained for a longer period before the solidifying layer finally arrests the spread. For lesser amounts of latent heat, a lesser amount of energy transfer needs to take place for solidification to begin and the motion of leading edge of the droplet is inhibited by the faster solidification process.

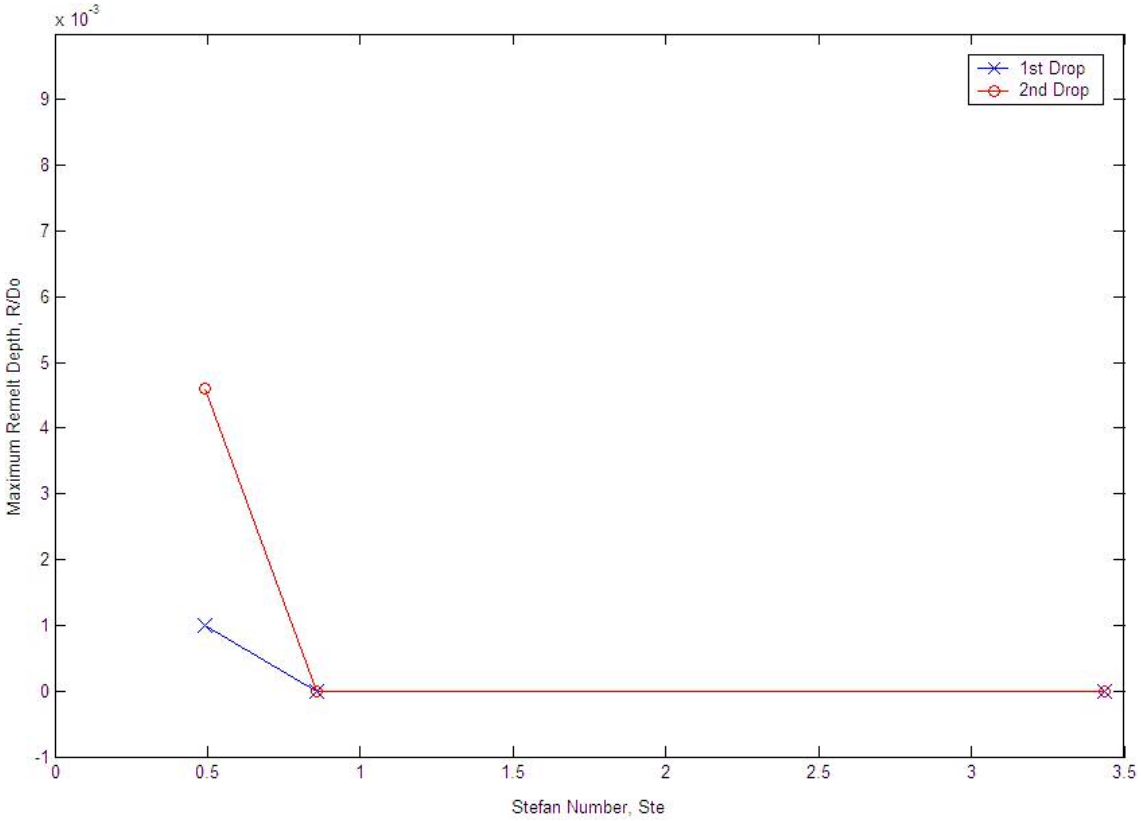

Figure 4.14 Variation of maximum remelt depth with latent heat

The influence of latent heat on the maximum depth of remelting, R, is illustrated in Figure 4.14. A small amount of remelting is observed when L = 104125 J/kg (Ste = 0.491), for both droplets. For the standard case (Ste = 0.859), and for the case where L = 14875 J/kg (Ste = 3.437), no remelting is found to occur.

4.3 Effect of Stefan Number

Finally, an investigation is conducted to reveal whether or not in fact, the Stefan number drives the spreading process in homologous deposition. As presented earlier in this chapter, studies were performed to understand individually, the influence of substrate temperature and latent heat on the spreading behavior of two molten tin droplets impinging onto a substrate of the same material. The Stefan number was used,

varying the substrate temperature while maintaining the latent heat as constant, and then varying the latent heat while maintaining the substrate temperature as constant. To determine whether there is a direct correlation between the Stefan number and the spread factor, a study was conducted over a wide range of values for the Stefan number, as shown in Table 4.1. The results are shown in Figure 4.15.

Table 4.1 Range of Stefan Numbers

Initial Substrate Temperature, in K	Latent Heat, in J/kg	Stefan Number
425	59500	0.347
400	59500	0.452
303	104125	0.491
375	59500	0.557
303	89250	0.573
350	59500	0.662
303	74735	0.684
325	59500	0.767
303	59500	0.859
303	44625	1.146
303	29750	1.718
303	14875	3.437

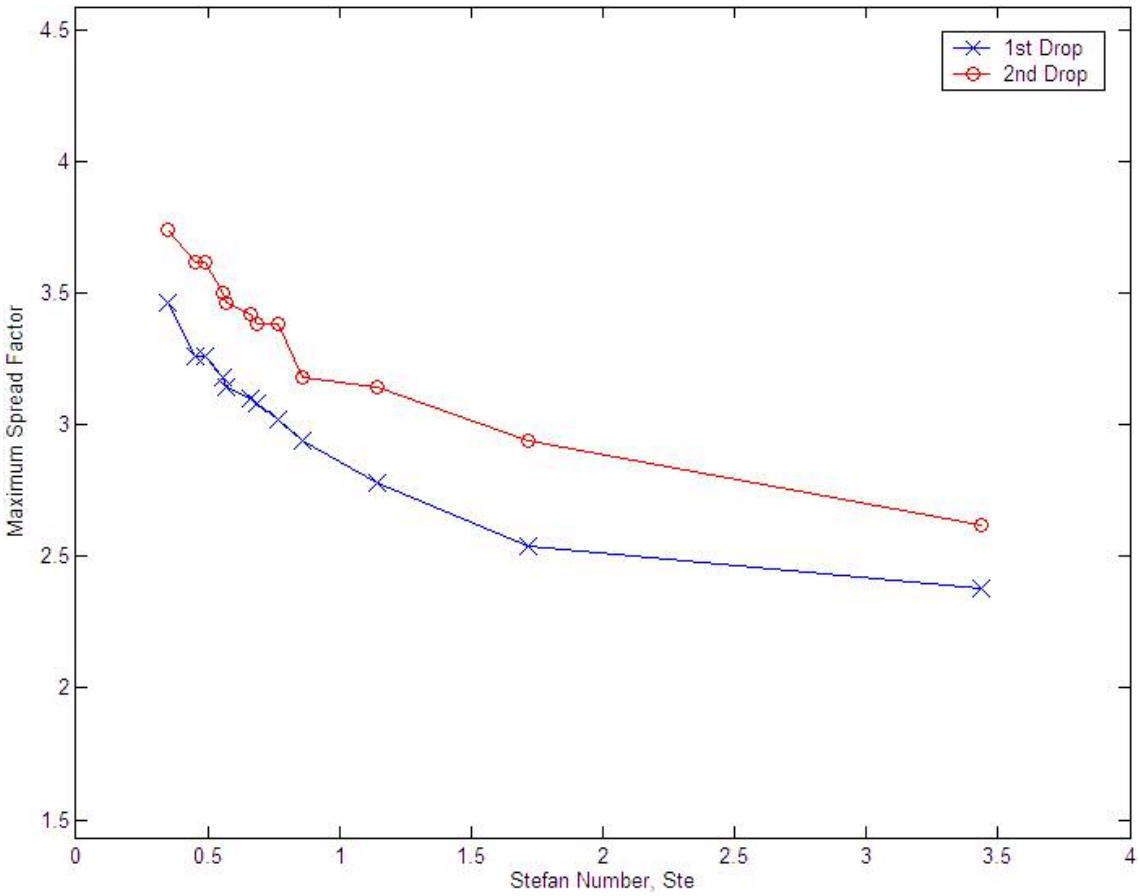

Figure 4.15 Effect of Stefan number on the maximum spread factor

It is evident that there exists a direct correlation between the Stefan number and the spread factor. A similar conclusion was made by Schiaffino et al. [20] in an earlier study focusing on single droplet impingement. From the above figure however, it is clear that Stefan number drives the spreading of droplets, resulting from the impingement of both the first and second droplet on a substrate of the same material.

CHAPTER V

CONCLUSION

5.1 Summary

The problem of sequential impingement of two molten tin droplets on a tin substrate has been studied and the spreading, solidification and remelting behavior exhibited by the droplets has been numerically investigated. The motivation behind the study is its ultimate application to developing an improved understanding of the overall deposition process to facilitate the enhancement of existing manufacturing technologies.

The mathematics behind the numerical model is presented in brief, for completeness. The fluid-flow solver RIPPLE is modified to incorporate modeling of heat transfer effects, and enable simulations of multiple droplet impingement onto a substrate. The assumptions and limitations of the model are enumerated. These do not, however, undermine the ability of the model to accurately analyze the aforementioned problem.

The formulation of the grid and the factors involved in the selection of the grid spacing are discussed. The results of the grid-sensitivity study are obtained, on the basis of which a uniform grid-spacing of 0.01 mm is selected for the study. An overview of the 'input file' that is required as the input to the flow solver is presented. The parameters employed in the standard case are tabulated and explained in brief. Parametric studies are conducted and compared with the standard case.

The simulation of the standard case is carried out and a chronological progression of the impact and solidification process is presented. It is observed that solidification begins the instant the droplet impinges onto the substrate. The solidification and spreading timescales are found to be of the same order, thus invalidating the assumption that solidification occurs after the droplet has completed the spreading process. The temperature contours in the substrate after impact of the first and second droplets are illustrated. It can be easily inferred that the conduction into the substrate is both axial and radial, and the assumption of one-dimensional conduction is inadequate and would result in over-simplification.

The effects of initial droplet temperature T_d, initial substrate temperature $T_{p,}$ and latent heat L, on the spreading, solidification and remelting phenomena are studied. Each of the phenomena is characterized by the maximum spread factor ξ, solidification time, and maximum remelt depth R respectively. The superheat parameter SHP, is used to illustrate the effect of T_d, and the Stefan number Ste is used to illustrate the effect of T_p and L, on the three phenomena.

The solidification time, maximum spread factor and maximum remelt depth are found to increase with increase in T_d. This behavior is attributed to the increased thermal energy associated with a droplet at a higher initial temperature. Uniform flow characteristics and a small amount of remelting are desired to obtain adequate bonding between splat and substrate. However, for higher initial droplet temperatures, a pit formation in the substrate is observed, which is undesirable. Although an increase in T_d

promotes substrate remelting, the amount of superheat must be carefully controlled to avoid excessive remelting.

An increase in T_p also results in an increase in the maximum spread factor and solidification time. The final splat shapes appear more uniformly spread. No remelting of the substrate by the either the first or second droplet is observed when the substrate is initially at room temperature. For $T_p > 303$ K, a small amount of remelting is observed. Hence, it is concluded that an increase in substrate temperature results in an increase in the maximum remelt depth. It also promotes uniform spreading of the droplet over the substrate, which is desired.

The desire to investigate and clarify the influence of Stefan number on the various phenomena being studied, led to the parametric study of the effects of variation in latent heat. The solidification time and maximum spread factor are found to increase as the latent heat is increased. Remelting is observed only for the highest value of latent heat simulated, while the rest of the cases did not exhibit any remelting. Finally, the effect of Stefan number on the spread factor is studied over a range of values of the Stefan number. The plot of spread factor versus the Stefan number reveals the direct correlation between the two. This confirms the role the Stefan number plays in the spread of droplets involved in homologous deposition.

The above results compare well with those published in available literature for single droplet impingement. Experiments involving two droplet impingement were not found in previous studies, and the corresponding results obtained in this study therefore, are subject to verification.

5.2 Future Work

Research is an ongoing process and there is always scope for further improvement. Possible areas of focus are the numerical model itself, and investigation into related problems. Both aspects are inter-related, since improving the numerical model facilitates the study of related droplet deposition phenomena; certain aspects of the model, however, can be improved only by gaining a better understanding of the underlying behavior.

Enhancements to the numerical model involve eliminating current limitations to expand the scope of practical situations that can be modeled using the existing code. The ability to model different materials of droplet and substrate, variation in different properties due to temperature, high Reynolds number flow, phenomena such as splashing and formation of fingers and variable thermal contact resistance are some of the significant areas that require attention in the near future. Thermal contact resistance is a complex issue, the understanding of which is essential to enable its numerical modeling and can be attained only by further experimental and analytical investigations.

Other related problems involving droplet deposition include oblique multiple droplet impingement, i.e. droplets whose axis of impact are not the same, droplets impinging onto inclined or rough surfaces, and formation of satellites and fingers. The study of these problems demands a more robust three-dimensional model, which would require immense computer memory and resources. Nevertheless, advances in computing have facilitated the progress in modeling fluid flows with heat transfer and the future of research in this area is bright.

APPENDIX A

PROGRAM EXECUTION

Performing a simulation of any case presented in this study involves the preparation of an input file, the compilation of the subroutines to obtain the executable file, and the submission of all necessary files to the High Performance Computer (HPC) for processing. The HPC functions on a Unix based operating system. An understanding of Unix commands is essential to create and modify files, navigate through various directories, handle the submission of the input files and post-process the output files.

The input file contains all information necessary to supply the flow solver with data to model the given problem and simulate the fluid and thermodynamic behavior. Data pertaining to the fluid and thermal parameters, initial location of the free surface and substrate, attributes of the simulation such the time-step and boundary conditions are specified in the input file. The input file is named 'input'.

The executable file is compiled using the Fortan compiler into a single executable, most commonly named 'ripple'. If no changes are made to the subroutines of the flow-solver, then the compilation needs to be done just once. The same 'ripple' executable file may be copied to different directories and employed in the simulations. However, if changes are made to the subroutines, say for example to vary the frequency at which the datafiles are printed out, then the modified subroutines have to be recompiled to obtain the new 'ripple' executable file.

A third file called 'file_nam.dat' is required to specify the number of datafiles that will be printed out. The 'file_nam.dat' file passes this number to the executable file that terminates execution when this specified number equals the number of datafiles printed out. The time-step between subsequent printouts is specified in the input file.

Datafiles are files that contain information relating to the values of the VOF function, enthalpy, velocity, pressure etc. at all the grid points. Each datafile is named rippxx.dat where xx represents the order of the file in the sequence of datafiles printed out. Therefore, the first datafile is named ripp01.dat, the second ripp02.dat and so on. It may be noted that the first datafile stores information pertaining to the initial condition of the model being studied.

The three files – 'input', 'ripple' and 'file_nam.dat' are required to be present in the same directory. These three files are then submitted to any available slot in the alpha_long or alpha_debug queue on the HPC. The queue status may be determined using the 'bqueues' command. Each simulation is run as a batch job, and each job is required to have a job name, desired queue, and the names of the files being submitted to the HPC for processing. The jobs are submitted using the 'bsub' command, and the status of the job may be checked using the 'bjobs' command. Any job may be terminated by the 'bkill' command, referencing the job using either its job name (specified by the user) or job number (specified by the HPC).

As mentioned earlier, the output of the flow solver is a sequence of datafiles, each of which contain the values of variables at different time-steps. These datafiles are post-processed using MATLAB. This software enables the plotting of various graphs presented in this study and also the animation of the impingement process. These graphs and animations help to better understand the phenomena of spreading, solidification and remelting during the impingement process.

APPENDIX B

INPUT FILE FOR STANDARD CASE

```
Droplet_impact (2 Droplet Standard Case Td=600 K Tp=303 K) [mm,ms,mg,K]
$numparam
        alpha = 1.0,
        autot = 1.0,
        conserve = .false.,
        delt = 1.0e-5,
        dtmax = 1.0e-3,
        twfin = 200000.0,
        con  =  0.3,
        fcvlim = 0.5,
        idiv = 1,
        dmpdt = 3000000.0,
        prtdt = 1000000.0,
        pltdt = 2.5e-2,
        sym = .true.,
        kt = 1,
        kb = 2,
        kl = 1,
        kr = 3,
$end
$fldparam
        gy = -9.81e-3,
        icyl = 1,
        isurf10 = 1,
        psat  =  0.0,
        xnu = 3.9e-4,
        rhof = 7.0,
        sigma = 0.621,
        vi = 3.0,
        cangleb = 45.0,
$end
$mesh
        nkx = 1,
        xl = 0.0,2.0,
        xc = 1.0,
        nxl = 100,
        nxr = 100,
        dxmn = 0.01,
        nky = 1,
        yl = 0.0,3.56,
        yc = 1.5,
        nyl = 150,
        nyr = 206,
        dymn = 0.01,
```

```
$end
$obstcl
        nobs = 0,
$end
$freesurf
        nfrsrf = 4,iequib = 0,
        fc1(1) = -2.0, ifh(1) = 1,
        fa1(2) =  0.0, fa2(2) = 1.0,
        fb1(2) = -6.6, fb2(2) = 1.0, fc1(2) = 10.8275, ifh(2) = 0,
        fa1(3) =  0.0, fa2(3) = 1.0,
        fb1(3) = -3.52, fb2(3) = 1.0, fc1(3) = 3.0351, ifh(3) = 0,
        fb1(4) = 1.0,  fc1(4) = -1.5,ifh(4) = 0,
$end
$graphics
        plots = .true., dump = .false.,
        iout =  0, 1, 0, 0, 0, 0, 0, 0, 0, 0, 0, 0, 0,
                0, 0, 0, 0, 0, 0, 0, 0, 0, 0, 0, 0, 0,
                0, 0, 0, 0, 0, 0, 0, 2,150, 0,-1, 0, 1, 0,
        iysymplt = 1,
$end
$heateq
        heat = .true.,
        ischeme = 3,
        tid = 600.0,
        tip = 303.0,
        tia = 303.0,
        cpp = 250.0,
        cpd = 250.0,
        cpa = 50.0,
        tkp = 63.9,
        tkd = 30.0,
        lhpc= 59500.0,
        hmr = 5.0,
        tl = 510.0,
        ts = 505.0,
        teps = 1.0e-8,
$end
```

APPENDIX C

MELTING FRONT PROPAGATION PLOTS

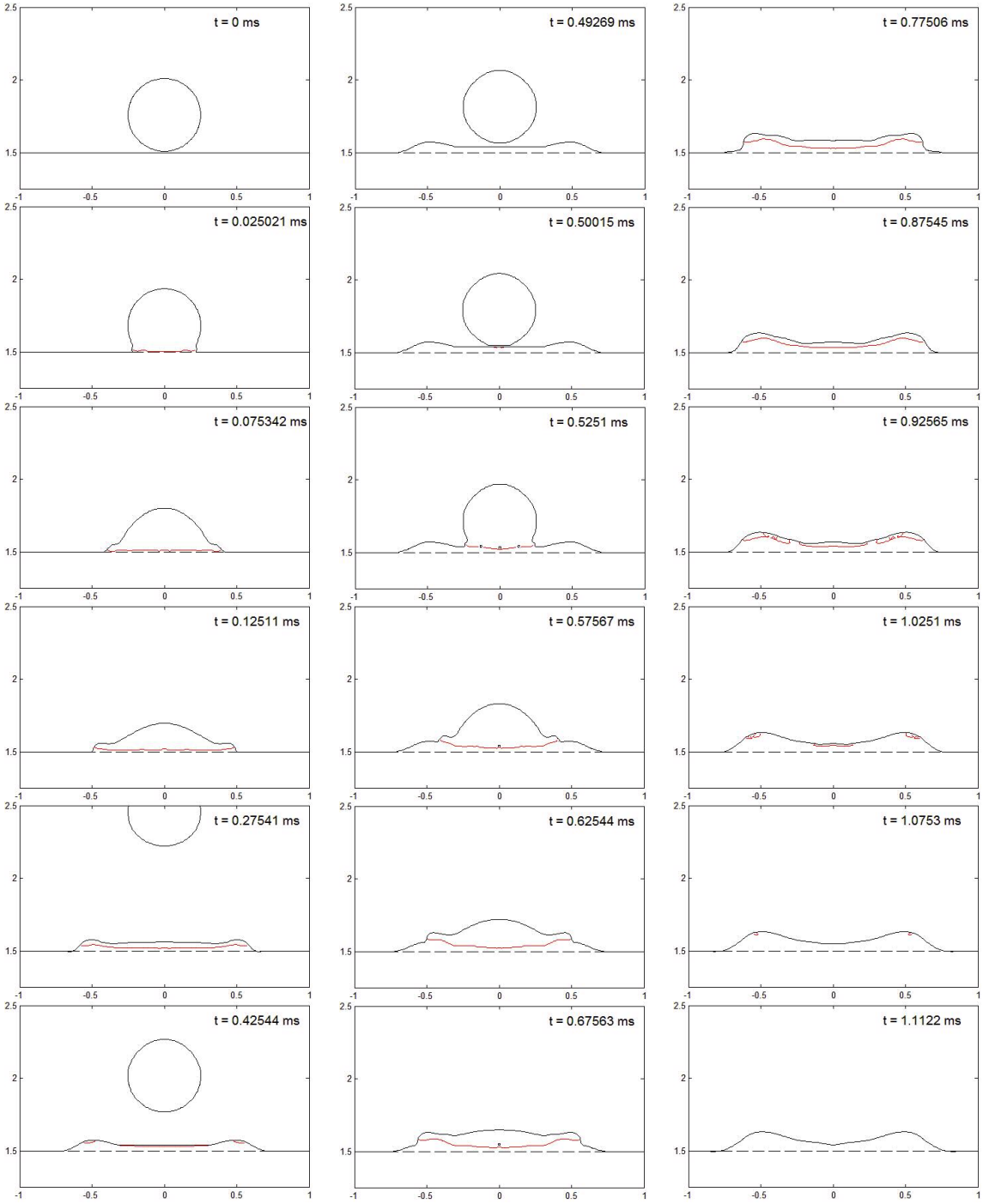

$T_d = 550$ K, $T_p = 303$ K, L = 59500 J/kg

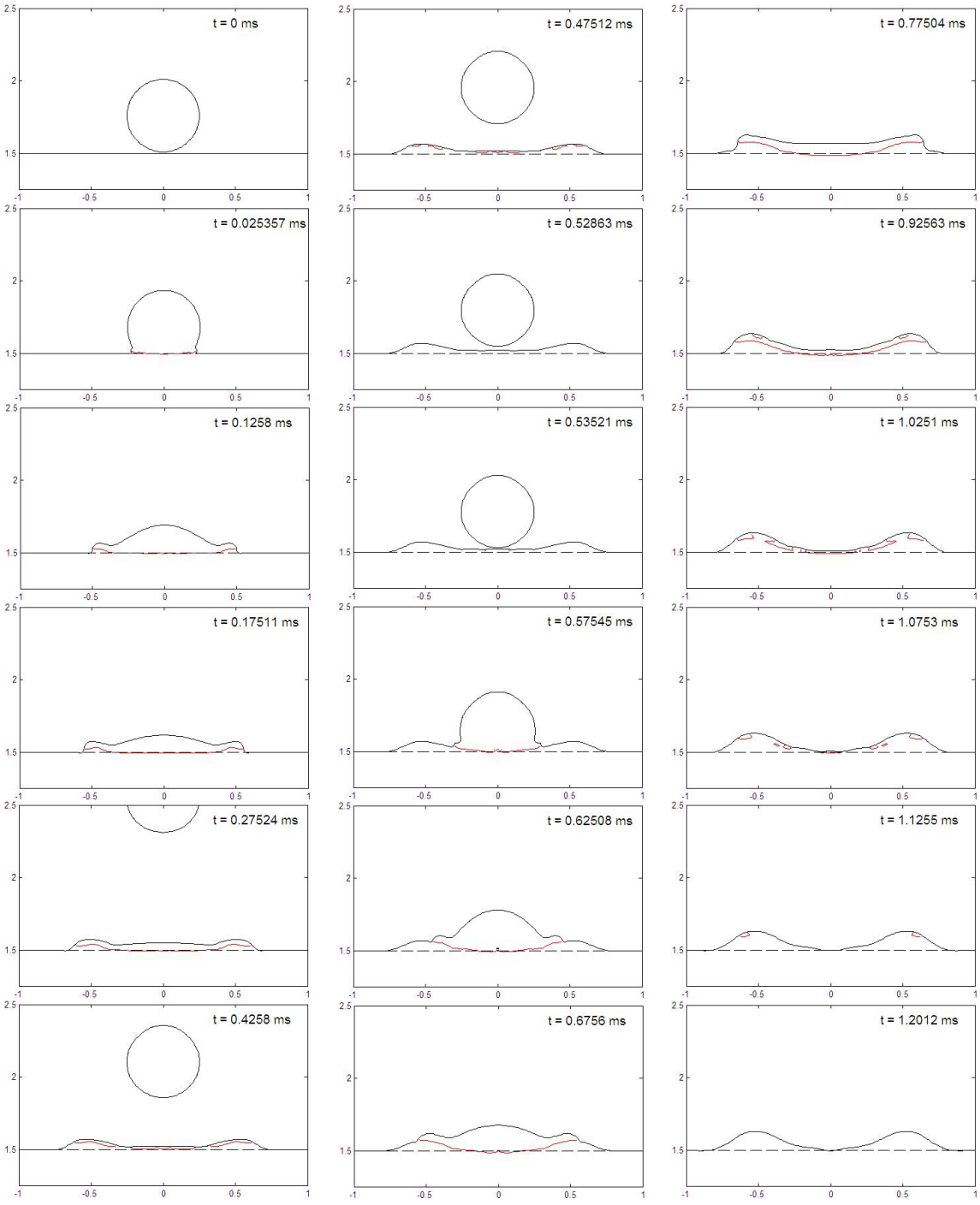

$T_d = 650$ K, $T_p = 303$ K, L = 59500 J/kg

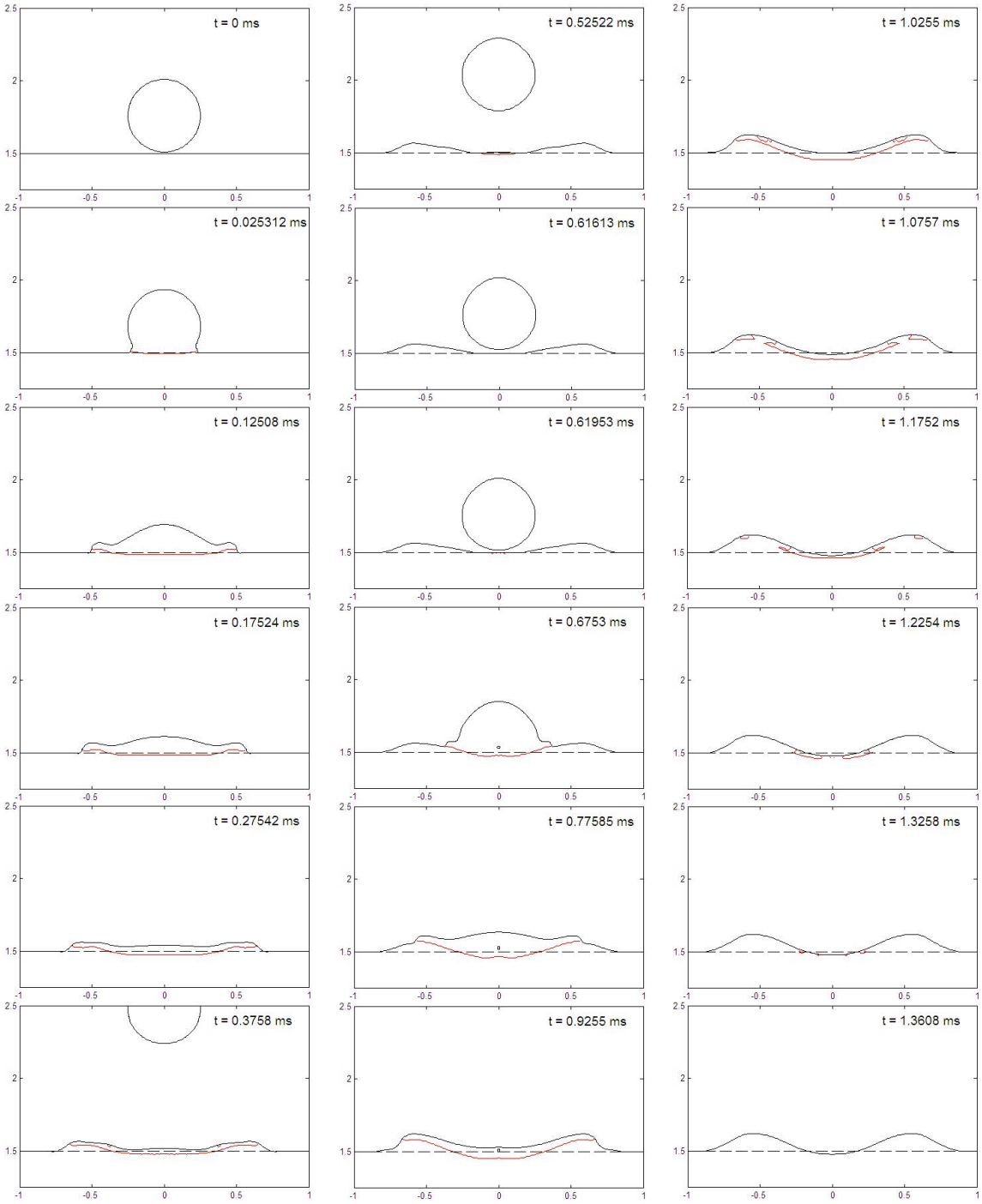

$T_d = 750$ K, $T_p = 303$ K, L = 59500 J/kg

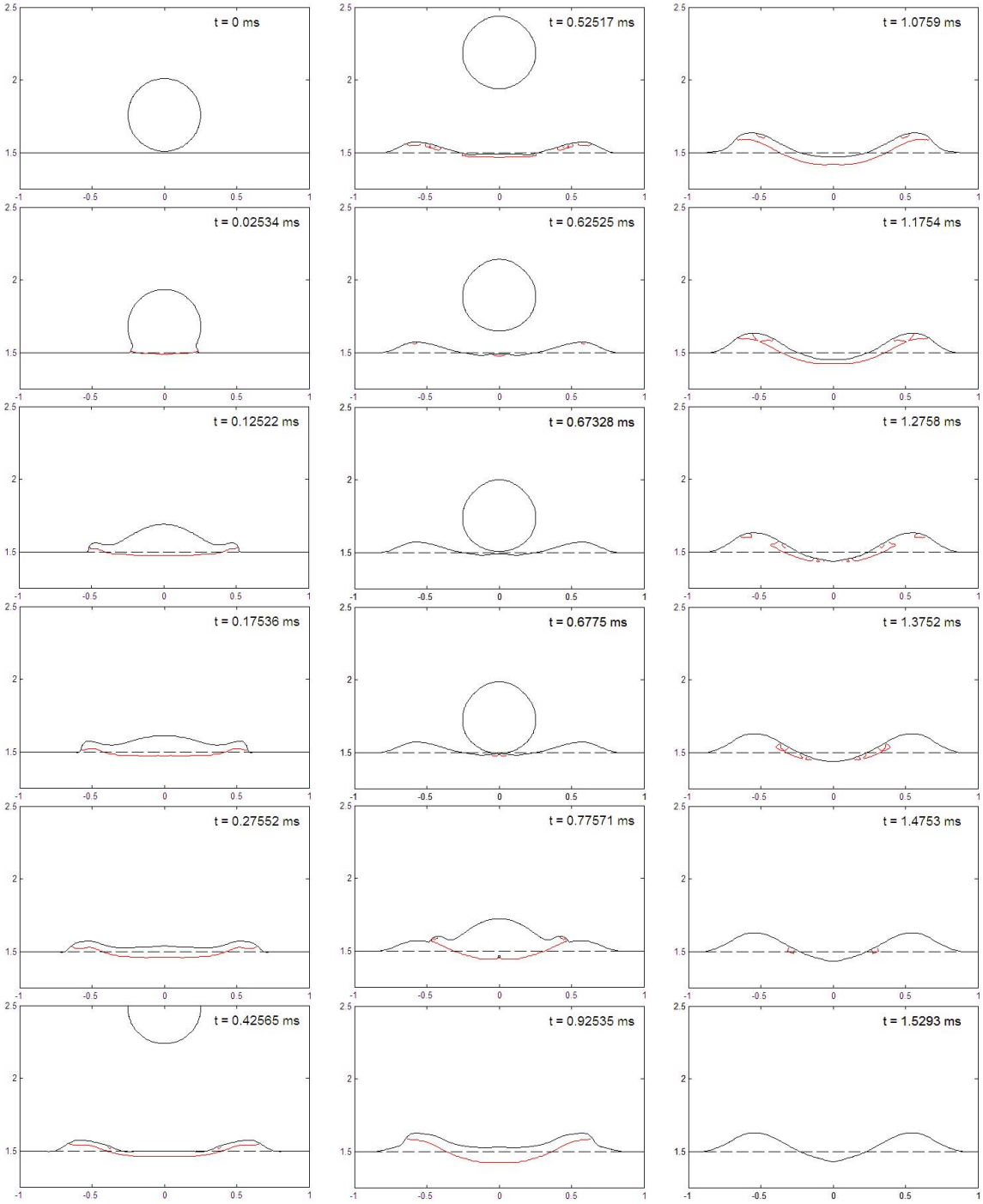

$T_d = 850$ K, $T_p = 303$ K, L = 59500 J/kg

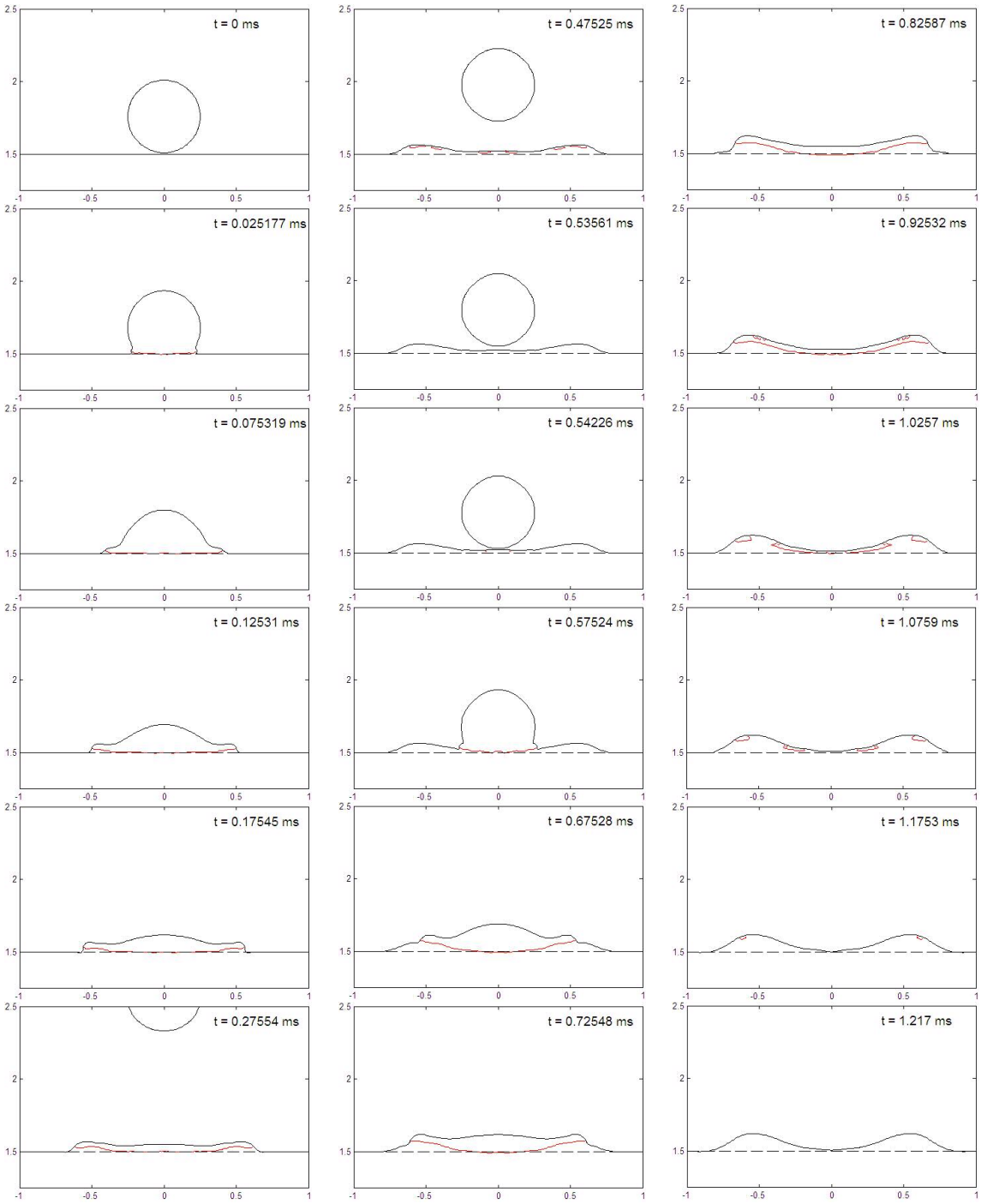

$T_d = 600$ K, $T_p = 350$ K, L = 59500 J/kg

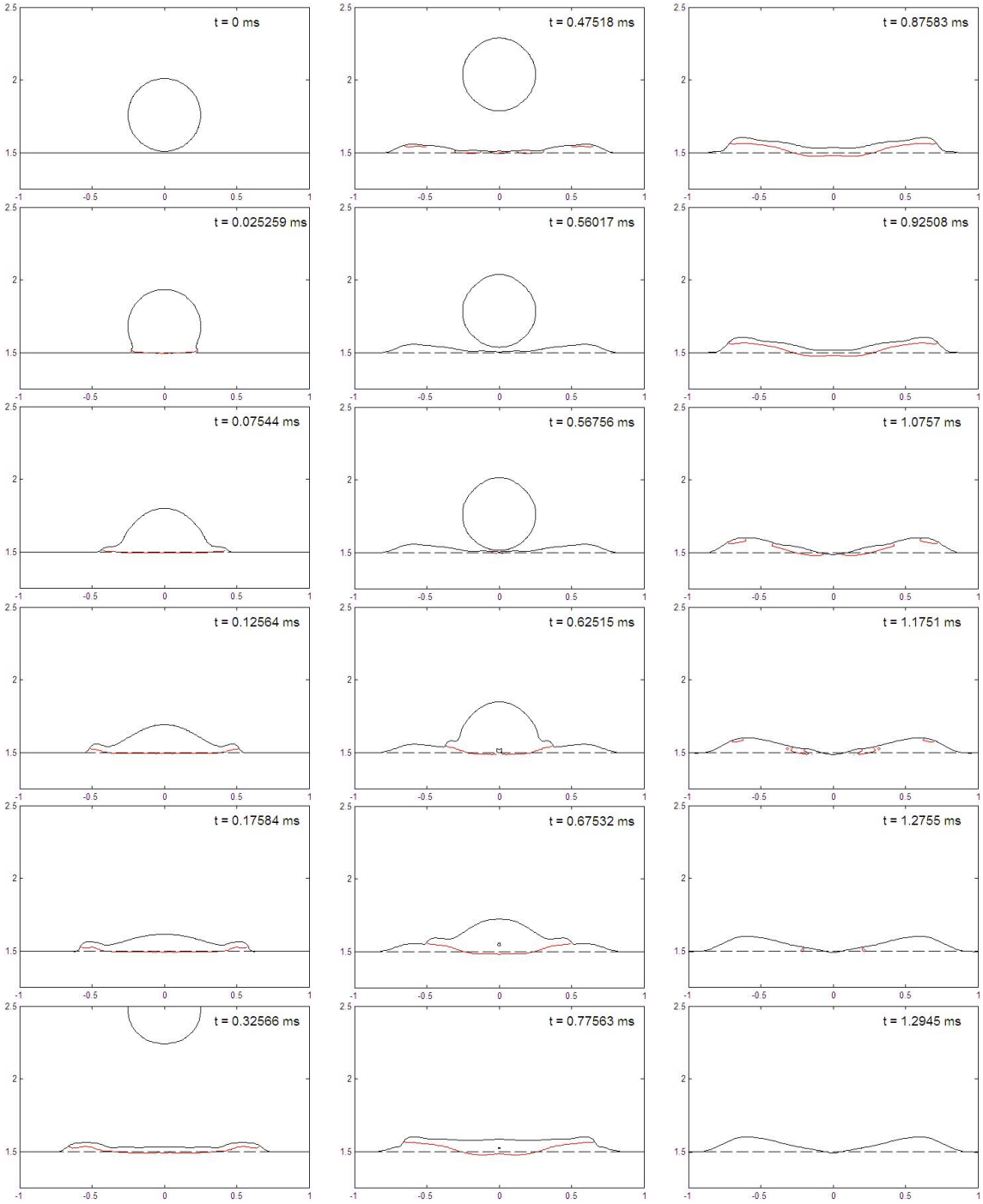

$T_d = 600$ K, $T_p = 400$ K, L = 59500 J/kg

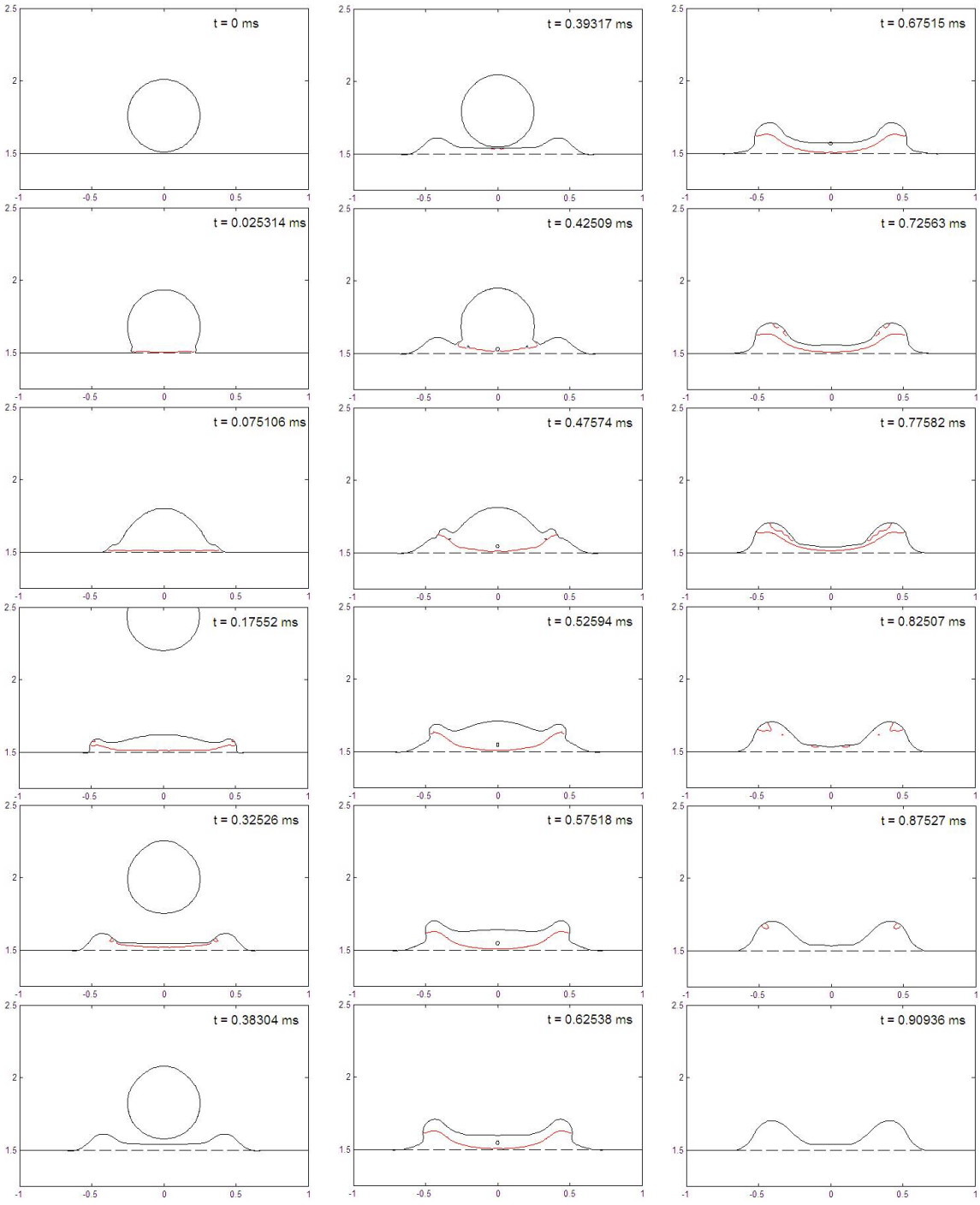

$T_d = 600$ K, $T_p = 303$ K, L = 14875 J/kg

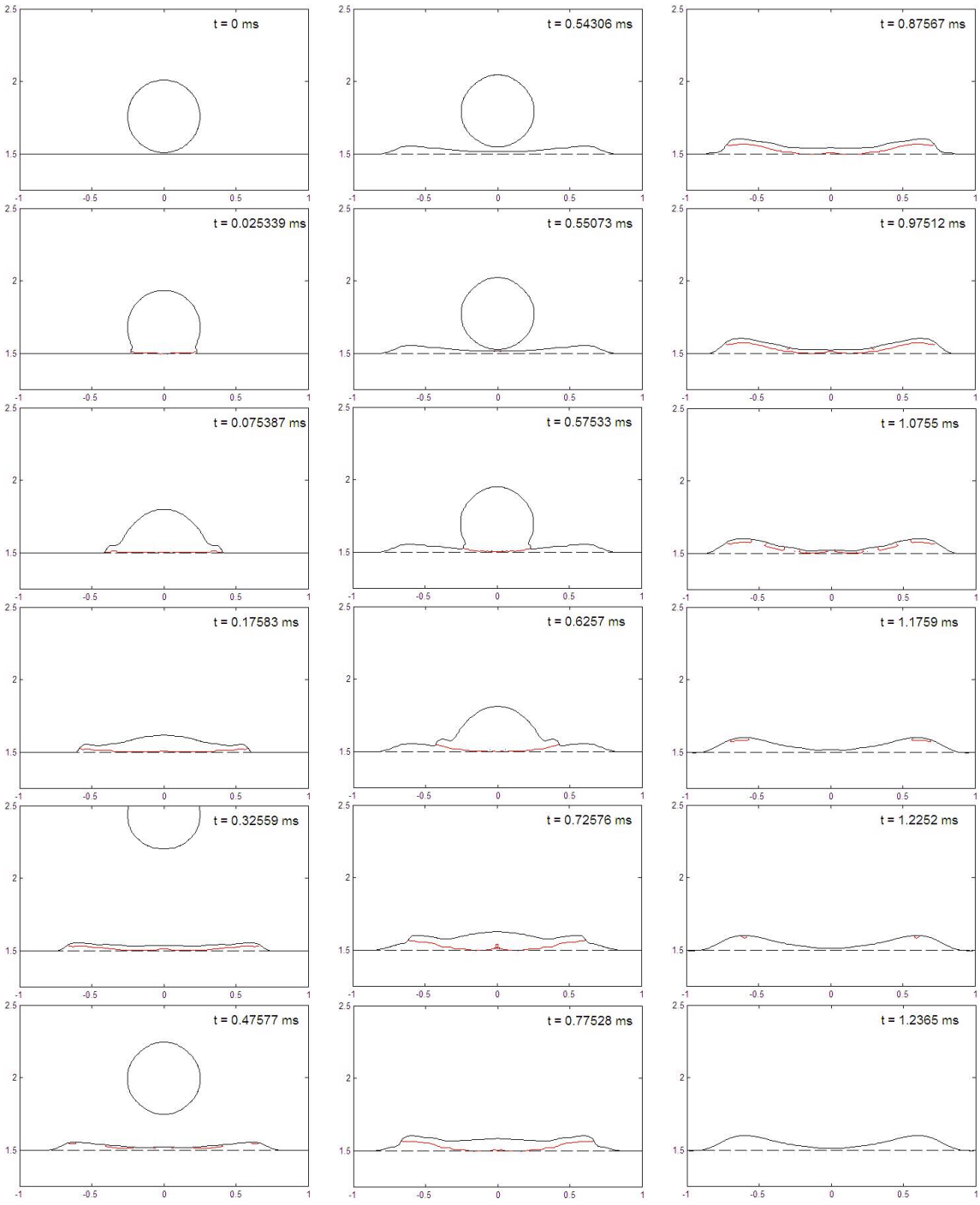

$T_d = 600$ K, $T_p = 303$ K, L = 104125 J/kg

REFERENCES

[1] Amon, C. H., Schmaltz, K. S., Merz, R. & Prinz, F. B. (1996). Numerical and experimental investigation of interface bonding via substrate remelting of an impinging molten metal droplet. Transactions of the ASME: Journal of Heat Transfer, 118, 164-171.

[2] Zarzalejo, L. J., Schmaltz, K. S. & Amon, C. H. (1999). Molten droplet solidification and substrate remelting in microcasting Part I: numerical modeling and experimental verification. Heat and Mass Transfer, 34, 477-485.

[3] Zhao, Z., Poulikakos, D. & Fukai, J. (1996). Heat transfer and fluid dynamics during the collision of a liquid droplet on a substrate – I. Modeling. International Journal of Heat and Mass Transfer, 39 (13), 2771-2789.

[4] Attinger, D., Zhao, Z. & Poulikakos, D. (2000). An experimental study of molten microdroplet surface deposition and solidification: transient behavior and wetting angle dynamics. Transactions of the ASME: Journal of Heat Transfer, 122, 544-556.

[5] Haferl, S. & Poulikakos, D. (2002). Transport and solidification phemonema in molten microdroplet pileup. Journal of Applied Physics, 92 (3), 1675-1689.

[6] Sampath, S. & Jiang, X. (2001). Splat formation and microstructure development during plasma spraying: deposition temperature effects. Material Science and Engineering A304-306, 144-150.

[7] Mehdizadeh, N. Z., Chandra S. & Mostaghimi, J. (2003). Adhesion of tin droplets impinging on a stainless steel plate: effect of substrate temperature and roughness. Science and Technology of Advanced Materials, 4, 173-181.

[8] Gao, F. & Sonin, A. A. (1994). Precise deposition of molten microdrops: the physics of digital microfabrication. Proceeding of the Royal Society of London, A, 533-554.

[9] Priest, J. W., Bordett, H., Smith, C. V., DuBois, P. N., Vanacek, D. G. & Holt, B. R. (1993). Liquid metal-jetting: its application to SMT. Journal of Surface Mount Technology, 6 (5), 4-9.

[10] Holt, B. R. (1995). The normal incident impact phenomena and solidification of a liquid metal droplet onto a rigid substrate. Ph.D. Thesis, Department of Mechanical & Aerospace Engineering, University of Texas at Arlington.

[11] Liu, Q. & Orme, M. (2001). On precision droplet-based net-from manufacturing technology. Proceedings of the Institution of Mechanical Engineers, 215 (B), 1333-1355.

[12] Madejski, J. (1976). Solidification of droplets on a cold surface. International Journal of Heat and Mass Transfer, 19, 1009-1013.

[13] Madejski, J. (1983). Droplets on impact with solid surface. International Journal of Heat and Mass Transfer, 26 (7), 1098-1102.

[14] Collings, E. W., Markworth, A. J., McCoy, J. K. & Saunders, J. H. (1990). Splat-quench solidification of freely falling liquid-metal drops by impact on a planar substrate. Journal of Material Science, 25, 3677-3682.

[15] Trapaga, G., Matthys, E. F., Valencia, J. J. & Szekely, J. (1992). Fluid flow, heat transfer and solidification of molten metal droplets impinging on substrates: comparison of numerical and experimental results. Metallurgical Transactions B, 23B, 701-718.

[16] Bennett, T. & Poulikakos, D. (1993). Splat-quench solidification: estimating the maximum spreading of a droplet impacting a solid surface. Journal of Materials Science, 28, 963-970.

[17] Liu, H., Lavernia, E. J. & Rangel, R. H. (1993). Numerical simulation of substrate impact and freezing of droplets in plasma spray processes. Journal of Physics D: Applied Physics, 26, 1900-1908.

[18] Kang, B., Zhao, Z. & Poulikakos, D. (1994). Solidification of liquid metal droplets impacting sequentially on a solid surface. Transactions of the ASME: Journal of Heat Transfer, 116, 436-445.

[19] Kang, B., Waldvogel, J. & Poulikakos, D. (1995). Remelting phenomena in the process of splat solidification. Journal of Materials Science, 30, 4912-4925.

[20] Schiaffino, S. & Sonin, A. A. (1997). Molten droplet deposition and solidification at low Weber numbers. Physics of Fluids, 9 (11), 3172-3187.

[21] Chin, R. K., Beuth, J. L. & Amon, C. H. (1996). Thermomechanical modeling of molten metal droplet solidification applied to layered manufacturing. Mechanics of Materials, 24, 257-271.

[22] Schmaltz, K. S., Zarzalejo, L. J. & Amon, C. H. (1999). Molten droplet solidification and substrate remelting in microcasting Part II: parametric study and effect of dissimilar materials. Heat and Mass Transfer, 35, 17-23.

[23] Zhao, Z., Poulikakos, D. & Fukai, J. (1996). Heat transfer and fluid dynamics during the collision of a liquid droplet on a substrate – II. Experiments. International Journal of Heat and Mass Transfer, 39 (13), 2791-2802.

[24] Rangel, R. H. & Bian, X. (1997). Metal-droplet deposition model including liquid deformation and substrate remelting. International Journal of Heat and Mass Transfer, 40 (11), 2549-2564.

[25] Tong, A. Y. & Holt, B. R. (1997). A numerical study on the solidification of liquid metal droplets impacting onto a substrate. Numerical Heat Transfer, Part A, 31, 797-817.

[26] Lu, M. (2000). Numerical modeling of multi-phase surface flow. Ph.D. Thesis, Department of Mechanical & Aerospace Engineering, University of Texas at Arlington.

[27] Dheenakumar, V. (2003). Solidification of an impinging molten droplet with substrate remelting. M.S. Thesis, Department of Mechanical & Aerospace Engineering, University of Texas at Arlington.

[28] Pasandideh-Fard, M., Chandra, S. & Mostaghimi, J. (2002). A three-dimensional model of droplet impact and solidification. International Journal of Heat and Mass Transfer, 45, 2229-2242.

[29] Fukai, J., Ozaki, T., Asami, H. & Miyatake, O. (2000). Numerical simulation of liquid droplet solidification on substrates. Journal of Chemical Engineering of Japan, 33 (4), 630-677.

[30] Attinger, D. & Poulikakos, D. (2001). Melting and resolidification of a substrate caused by molten microdroplet impact. Transactions of the ASME: Journal of Heat Transfer, 123, 1110-1122.

[31] Welch, J. E., Harlow, F. H., Shannon, J. P. & Daly, B. J. (1966). The MAC method, Los Alamos Scientific Laboratory Report LA-3425, Los Alamos, New Mexico.

[32] Hirt, C. W., Nichols, B. D. & Romero, N. C. (1975). SOLA - A numerical solution algorithm for transient fluid flows, Los Alamos Scientific Laboratory Report LA-5852, Los Alamos, New Mexico.

[33] Hirt, C. W., Nichols, B. D., & Romero, N. C. (1980). SOLA-VOF- A solution algorithm for transient fluid flows with multiple free boundaries, Los Alamos Scientific Laboratory Report LA-8355, Los Alamos, New Mexico.

[34] Torrey, M. D., Cloutman, L. D., Mjolsness, R. C. & Hirt, C. W. (1985). NASA-VOF2D: A computer program for incompressible flows with free surfaces, Los Alamos Scientific Laboratory Report LA-10612, Los Alamos, New Mexico.

[35] Kothe, D. B., Mjolsness, R. C. & Torrey, M. D. (1991). RIPPLE: A computer program for incompressible flows with free surfaces, Los Alamos National Laboratory Report LA-12007- MS, Los Alamos, New Mexico.

[36] Brackbill, J. U., Kothe, D. B. & Zemach, C. (1992) A continuum method for modeling surface tension, Journal of Computational Physics, 100, 335-354.

[37] Kershaw, D. S. (1978). The incomplete Cholesky-conjugate gradient method for the iterative solution of systems of linear equations. Journal of Computational Physics, 26, 43-65.

[38] Samarskii, A. A., Vabishchevich, P. N., Iliev, O. P. & Churbanov, A. G. (1993). Numerical simulation of convection/diffusion phase change problems - a review. International Journal of Heat and Mass Transfer, 36 (17), 4095-4106.

[39] Hirt, C. W. & Nichols, B. D. (1981). Volume of fluid (VOF) method for the dynamics of free boundaries. Journal of Computational Physics, 39, 201-225.

[40] Youngs, D. L. (1982). Time-dependent multi-material flow with large fluid distortion. Numerical Methods for Fluid Dynamics, Academic, New York, 273-285.

[41] Rudman, M. (1997). Volume-tracking methods for interfacial flow calculations. International Journal for Numerical Methods in Fluids, 24, 671-691.

[42] Voller, V.R. & Swaminathan, C.R. (1990). Fixed grid techniques for phase change problems: a review. International Journal for Numerical Methods in Engineering, 30, 875-898.

[43] Tong, A.Y. (2003). A numerical study on the hydrodynamics and heat transfer of a circular liquid jet impinging onto a substrate. Numerical Heat Transfer, Part A, 44, 1-19.

[44] Tong, A. Y. (2003). Impingement heat transfer of free-surface liquid jets with phase change at the substrate. The 6th ASME-JSME Thermal Engineering Joint Conference, TED-AJ03-272.

BIOGRAPHICAL INFORMATION

Lister Manohar Pinto graduated from the Manipal Institute of Technology (MIT), Manipal, India, in 2002 with a Bachelors degree (B.E.) in Mechanical Engineering, securing the first rank in his senior year. He was the recipient of the second prize in the annual mechanical engineering project exhibition organized at MIT in the same year. He joined the University of Texas at Arlington in August 2003, and was the recipient of a Fellowship awarded by the Department of Mechanical & Aerospace Engineering. His research interests include numerical heat transfer and fluid dynamics. He is an active member of Tau Beta Pi, Texas Eta Chapter, a recognized engineering honor society. He graduated with his Master of Science degree in Mechanical Engineering in August 2005, with a G.P.A of 4.0.